2011

Tidal modulation on the Changjiang River plume in summer

Hui Wu
East China Normal University

Jianrong Zhu
East China Normal University

Jian Shen
Virginia Institute of Marine Science, shen@vims.edu

Harry V. Wang
Virginia Institute of Marine Science, wang@vims.edu

Tidal modulation on the Changjiang River plume in summer

Hui Wu,[1] Jianrong Zhu,[1] Jian Shen,[2] and Harry Wang[2]

Received 8 April 2011; revised 8 May 2011; accepted 23 May 2011; published 20 August 2011.

[1] Tide effects on the structure of the near-field Changjiang River plume and on the extension of the far-field plume have often been neglected in analysis and numerical simulations, which is the focus of this study. Numerical experiments highlighted the crucial role of the tidal forcing in modulating the Changjiang River plume. Without the tidal forcing, the plume results in an unrealistic upstream extension along the Jiangsu coast. With the tidal forcing, the vertical mixing increases, resulting in a strong horizontal salinity gradient at the northern side of the Changjiang River mouth along the Jiangsu coast, which acts as a dynamic barrier and restricts the northward migration of the plume. Furthermore, the tidal forcing produces a bidirectional plume structure in the near field, and the plume separation is located at the head of the submarine canyon. A significant bulge occurs around the head of the submarine canyon and rotates anticyclonically, which carries a large portion of the diluted water toward the northeast and merges into the far-field plume. A portion of the diluted water moves toward the southeast, which is mainly caused by tidal rectification. This bidirectional plume structure is more evident under certain wind conditions. During the neap tide with the reduced tidal energy, the near-field plume extends farther offshore, and the bulge becomes less evident. These dynamic behaviors are maintained and are fundamentally important in the region around the river mouth even under the summer monsoon and the shelf currents, although in the far field the wind forcing and shelf currents eventually dominate the plume extension.

Citation: Wu, H., J. Zhu, J. Shen, and H. Wang (2011), Tidal modulation on the Changjiang River plume in summer, *J. Geophys. Res.*, *116*, C08017, doi:10.1029/2011JC007209.

1. Introduction

[2] Summer extension of the Changjiang River plume is one of the most important physical processes in the Yellow and East China Seas (YECS) [e.g., *Chen et al.*, 2008; *Mao et al.*, 1963; *Moon et al.*, 2010; *Zhu et al.*, 1997]. The Changjiang River accounts for the largest source of freshwater and nutrient loadings into the West Pacific (Figure 1). Annually it discharges 9.24×10^{11} m^3 of freshwater into the YECS, and the fluvial flow rate can reach 50,000 to 60,000 m^3 s^{-1} in summer [*Shen et al.*, 2003]. The spatial distribution of higher chlorophyll *a* concentration corresponds well with the distribution of low-salinity Changjiang diluted water [*Kim et al.*, 2009]. Emanating from the river mouth, the Changjiang River plume floats over the ambient ocean water and forms a strong stratification that is thought to be a major factor causing one of the largest hypoxia regions in the world [*Li et al.*, 2002; *Rabouille et al.*, 2008]. In winter, the Changjiang River plume spreads to the south along the Zhejiang coast as expected under the northerly winter monsoon. However, in summer, the Changjiang River plume turns to the northeast [*Mao et al.*, 1963]. The diluted water can even extend to Jeju Island, which is about 450 km away from the river mouth, and can cause a massive fish mortality in that region [*Moon et al.*, 2009].

[3] The southerly summer monsoon is found to be the dominant factor that causes such a northeastward extension [*Chang and Isobe*, 2003; *Zhu et al.*, 1997]. When the southerly wind speed exceeds 3 m s^{-1}, the extension of the Changjiang River plume will be altered to the northeast due to Ekman transport [*Zhu et al.*, 1997]. The far-field diluted water joins the northeastward shelf currents system and flows out of the YECS region through the Tsushima-Korea Strait, where the year-round freshwater outflow was estimated to be at least 70% of the total Changjiang discharge [*Chang and Isobe*, 2003; *Isobe et al.*, 2002].

[4] However, the plume pattern is highly variable in a large region near the Changjiang River mouth. Although the Changjiang diluted water will eventually spread to the northeast under the influence of southerly summer monsoon, the underlying mechanisms controlling its initial stage and the near field variation is still obscure. The southerly wind [*Zhu et al.*, 1997], the huge Changjiang runoff in summer [*Le*, 1984], the vortex stretching that resulted from the increased depth offshore [*Beardsley et al.*, 1985], the basin-scale secondary cyclonic flow produced by the cold water dome in the Yellow Sea [*Zhu et al.*, 1998] and the elevated sea surface that result from the Taiwan warm current [*Zhao*, 1991] were

[1] State Key Laboratory of Estuarine and Coastal Research, East China Normal University, Shanghai, China.
[2] Virginia Institute of Marine Science, School of Marine Science, College of William and Mary, Gloucester Point, Virginia, USA.

0148-0227/11/2011JC007209

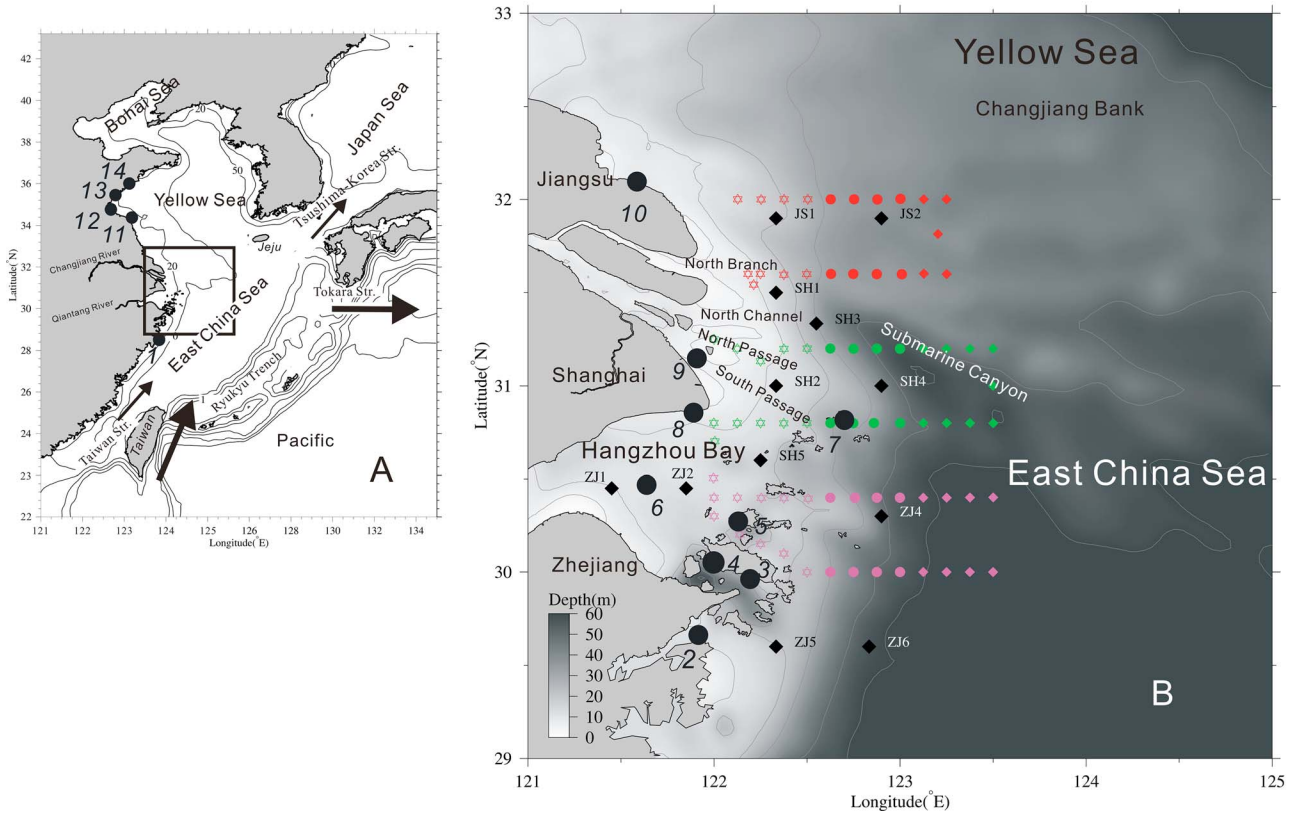

Figure 1. (a) Locations of the Changjiang River mouth, East China Sea, Yellow Sea, Bohai Sea, Japan Sea, and Pacific Ocean. Arrows overlaid are the inflow and outflow of the shelf currents. (b) Topography around the Changjiang River mouth. Black diamonds mark the locations for the shipped stations in November 2005. Colored symbols signify the cruising survey stations in August 2008. The black solid circles in Figures 1a and 1b are the locations of tide gauge stations.

all thought to be important. Based on the satellite images of surface suspended sediments concentration, *Pu et al.* [2002] reported that the distance and direction of the Changjiang River plume can be totally changed over a period from 1 week to 10 days.

[5] The recent study by *Gao et al.* [2009] highlighted the significant intratidal variability of the Changjiang River plume near the river mouth. Sampling at different tidal phases can result in a distinct salinity distribution. The frequent variation of the Changjiang River plume found by *Pu et al.* [2002] could also result from the tidal effect. Tidal energy in coastal regions is several orders higher than in the deep oceans. Due to the broad continental shelf in the YECS region, the tidal range of 5.0m around the Changjiang River mouth is considerable [*Shen et al.*, 2003]. The associated strong tidal current can cause significant turbulent mixing and residual currents, which should have deep impacts on the plume extension, especially since the region around the Changjiang River mouth is relatively shallow. *Zhu et al.* [1999] argued it might favor the Changjiang River plume rapidly spreading to every direction. *Moon et al.* [2010] found that the spring-neap variation of the tidal mixing can detach the diluted water from the Changjiang River plume at the slope region of the Changjiang Bank. Despite the success of the numerical model of *Moon et al.* [2010], its resolution is not fine enough to characterize the details of the Changjiang River plume near the river mouth, where the plume seems highly variable with the tide [*Gao et al.*, 2009] and has significant eddy structures due to the baroclinic instability [*Chen et al.*, 2008]. It is still unclear that how the tide modulates the Changjiang River plume especially in the near field, and this is the focus of this study.

[6] Studies in the other estuaries have provided some clues as to the important role of the tide. For example, *Guo and Valle-Levinson* [2007] found that the tidal mixing causes an intensified salinity gradient and thereby restricts the upstream extension (opposite to the propagation of coastally trapped waves) of the plume off the Chesapeake Bay. For the Changjiang case, it appears that model studies without the tide can also produce an overestimated northwestward plume along the Jiangsu coast. Offshore the Amazon, *Geyer* [1995] found the difference of tidal mixing between the spring and neap tides can significantly alter the position of the plume front. Compared to the spring tidal case, during the neap tide due to the reduced mixing and therefore the increased stratification, the bottom salinity front is more shoreward while the surface plume (as indicated by salinity 20 psu) moves nearly 30 km farther offshore. Tide-induced mixing accelerates the changing of the plume water into the ambient water [*MacCready et al.*, 2009]. With the strong tide around the Columbia River mouth, the tidally oscillated plume can cover 50%–100% of the recirculating plume (i.e., the "bulge") and sharpens the salinity front [*Horner-Devine et al.*, 2009], thereby favoring the release of internal waves

and the enhancement of vertical mixing [*Nash and Moum*, 2005]. *McCabe et al.* [2009] found that, in the very near field region, the initial outflow directions impact on the lateral spreading of the Columbia River plume considerably. Through an idealized numerical model, *Chao* [1990] suggested that the tidal effect can introduce a pair of counter-rotating eddies off the river mouth. The anticyclonic eddy is generally stronger than the cyclonic one due to the influence of the Earth's rotation.

[7] These studies of various estuaries highlight the fact that the tide can alter the plume's spreading direction [*Chao*, 1990; *Guo and Valle-Levinson*, 2007; *McCabe et al.*, 2009] and spreading distance [*Geyer*, 1995], sharpen the front [*Horner-Devine et al.*, 2009], and produce a secondary internal wave as well as augment the plume thickness [*Nash and Moum*, 2005]. For the Changjiang case, the role of the energetic tide in modulating the plume spreading has not been well explored. Because of the large domain and high variability of the plume, applying a numerical model is a suitable alternative that can overcome the difficulties in obtaining synoptic observations for such a large-scale estuary. According to the previous studies, the model used should include the shelf currents in the YECS region that is thought to be related to the extension of the Changjiang River plume [*Chang and Isobe*, 2003; *Zhao*, 1991; *Zhou et al.*, 2009]. Tide should also be included into the model for the reasons described above. The Changjiang estuary is bifurcated with complicated bathymetry. *Chen et al.* [2008] demonstrated that a high resolution is required to correctly simulate the Changjiang River plume, especially near the river mouth. The interaction between the shallow topography and the tide can produce a subtidal circulation that flows into the estuary through the South Passage and outflows through the North Channel, thus causing the freshwater to flow out more in the North Channel [*Wu et al.*, 2010]. Therefore, the extensive intertidal flat should be included and a wet/dry method should be employed in the model.

[8] In this study we established a high-resolution numerical model, which covers the entire YECS region, to investigate the physical mechanisms of the tidal modulation on the Changjiang River plume. The detailed description of our model can be seen in section 2. Several validations were introduced in section 3. Through additional experiments without the tidal forcing, we elucidated the key role of tide in correctly simulating the Changjiang River plume. In section 4, four process-oriented numerical experiments were presented and the physical mechanisms of how tide modulated the Changjiang River plume were discussed. Finally, summaries were drawn in section 5.

2. Methods

2.1. Numerical Model

[9] The hydrodynamic kernel of our model is the ECOM-si [*Blumberg*, 1994] that originated from the POM [*Blumberg and Mellor*, 1987] and later underwent several improvements by *Chen et al.* [2001] to address the demand of numerical simulations in the water bounded by a complicated coastline. The barotropic process was treated implicitly and thus allowed a bigger time step independent of the propagation of a gravity wave. A robust HSIMT-TVD advection scheme developed by *Wu and Zhu* [2010] was used to solve the transport equations. This scheme features third-order accuracy and can prevent numerical oscillations. Because the tide was included in the model and the grid resolution was high, the time step was significantly restricted by the maximum flood/ebb currents. To increase the model efficiency, the time step was set to vary automatically based on the CFL criterion and thus allowed the use of a larger time step during low-current periods but reduced the time step when the tidal current was large. The model used the modified Mellor and Yamada level 2.5 turbulent closure model [*Galperin et al.*, 1988; *Mellor and Yamada*, 1982]. For horizontal mixing, the parameterization method of *Smagorinsky* [1963] was used with a coefficient of 0.1. A wet/dry scheme was included using a critical depth of 0.25 m.

[10] The model domain covered the entire East China Sea, Yellow Sea, Bohai Sea, and parts of the Pacific Ocean and the Japan Sea (Figure 2). To reduce the numerical error that results from the σ transformation over the steep shelf break, the model bathymetry was cut at 1000 m, roughly an e-folding depth of the Kuroshio Current [*Chen et al.*, 2008]. The model grid mesh spanned 272 × 285 cell indices in the horizontal. The open boundary (the interior edge of the shadowed area in Figure 2) was roughly parallel to the Ryukyu Islands, and was also parallel to the cophase lines of the dominant tide constituents [*Choi*, 1980]. Besides, the open boundary was roughly perpendicular to the shelf currents flowing in/out this region (shown in Figure 1a). Such a setting can simplify the specification of open boundary conditions. The fan-shaped mesh can allow higher-resolution grids to be placed near the Changjiang River mouth while reducing the grid resolution near the open boundary. Off the river mouth, the model mesh was about 2 km × 3 km (in two directions) (Figure 3). The amplitude of the tidal current (U_{amp}) near the plume front was $O(1)$ m s^{-1} (from model results), resulting in a tidal excursion distance (approximately $U_{amp}\ T/\pi$ where T is the tidal period) of $O(14)$ km. Therefore, the mesh size was sufficiently smaller than the tidal excursion distance. *Chen et al.* [2008] suggested that there are baroclinically induced eddies around the Changjiang River plume with approximate diameters of 60 km, and our mesh size was less than 1/20 of this scale. Furthermore, the model mesh fit the coastline fairly well near the river mouth. In the Kuroshio region, the model resolution was approximate 7 km × 12 km, or roughly 1/12°, similar to many other models for the shelf currents simulations in the YECS region [e.g., *Moon et al.*, 2010]. Twenty σ layers were used in the vertical with refined upper layer thicknesses. For a typical depth of 30 m off the Changjiang River mouth, the upper 5 m of the water column had 8 layers. This allowed for resolving the vertical structure of the Changjiang River plume.

[11] The open boundary was driven by the shelf currents and the tide currents in the form of normal velocity:

$$V_{nomal} = V_{shelf\ current} + V_{tidal\ current} \quad (1)$$

For the shelf currents, two inflows, the Taiwan Warm Current (TWC) along the Taiwan Strait and the Kuroshio inflow at the east side of the Taiwan Island, as well as two outflows, including the Tsushima Warm Current (TSWC) into Japan Sea and the Kuroshio outflow along the Tokara Strait, were specified at the open boundary (Figure 1a). The

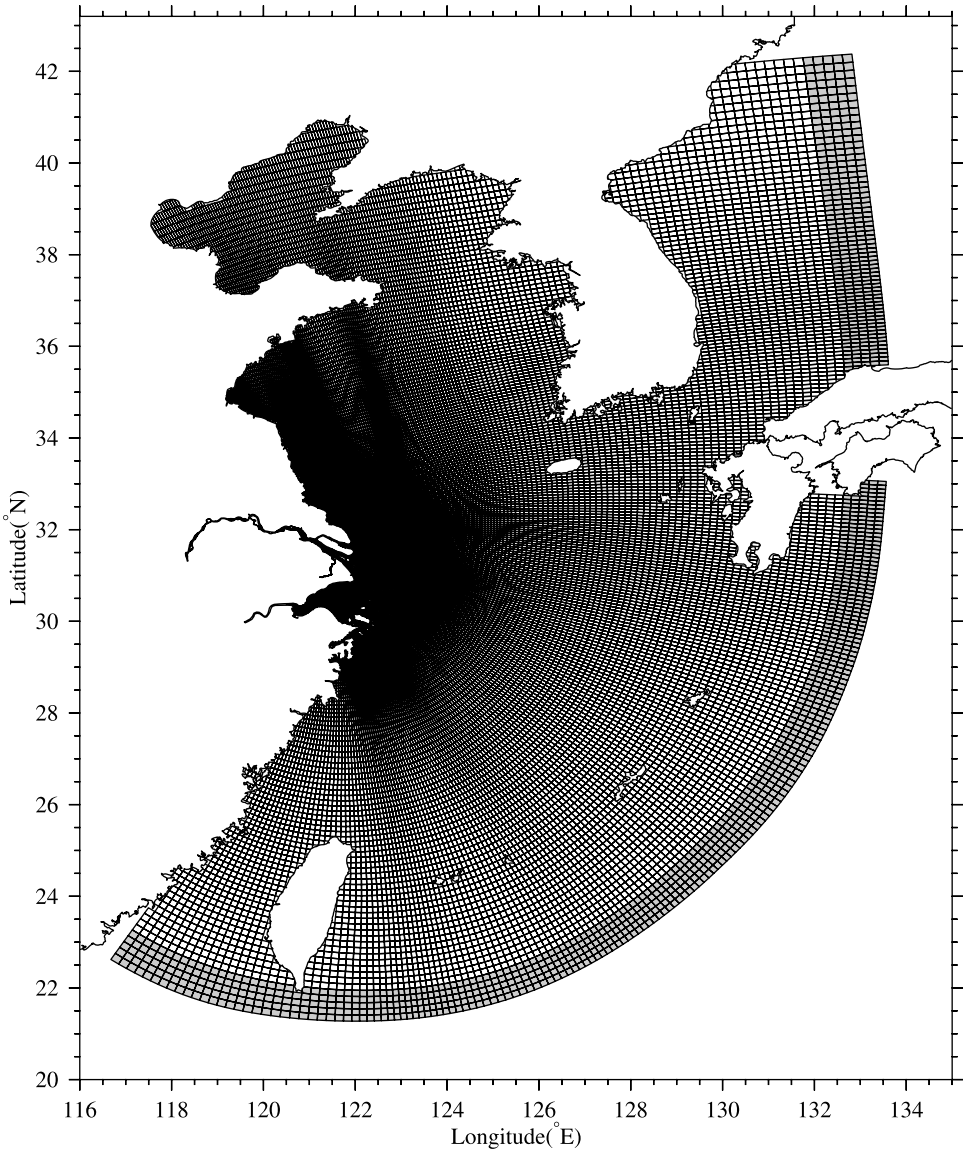

Figure 2. Numerical model mesh. The interior edge of the shadowed region is the open boundary for tidal and shelf currents. The exterior edge of the shadowed region is the open boundary for the model run driven by the tidal elevation.

monthly transports of the shelf currents were well documented by *Lee and Chao* [2003]. In August, for example, the TWC inflow is 2.4 Sv, the Kuroshio inflow is 28.0 Sv, the Kuroshio outflow is 26.74 Sv, and the TSWC outflow is 3.71 Sv. We superimposed the velocity on the open boundary by the assumption that it follows the parabolic distribution across the shelf currents axis both in the horizontal [*Lee and Chao*, 2003] and in the vertical. Given the width of the open boundary, the shelf currents, $V_{shelf\ current}$, can be determined. The width of the Kuroshio inflow was 108 km [*Lee and Chao*, 2003]. The width of the TWC was the same as that of the Taiwan Strait. The boundary of the TSWC was set at the Japan Sea, which provided some difficulties in determining the flow width. Here we used the entire Japanese Sea boundary as the flow width. However, it should be pointed out that alternative sets gave little difference in the shelf currents in the YECS region. A width close to that of the Tokara Strait was used for the Kuroshio outflow.

[12] For the tidal currents, we initially drove the model by 11 tidal constituents from the *NaoTide* data set (http://www.miz.nao.ac.jp/) at the exterior edge of the shadowed area (Figure 2) and stored the normal velocities at its interior edge. Then by using the harmonic analysis method, the harmonic constants of the tide current can be determined:

$$V_{tidal\ current} = \sum_{i=1}^{11} v_{amp} \cos(\omega_i t + g_i) \tag{2}$$

Surface heat flux was included in the model by the monthly data from NCEP (National Centers for Environmental Prediction). A bulk formula suggested by *Ahsan and Blumberg* [1999] was used to calculate the atmospheric radiation

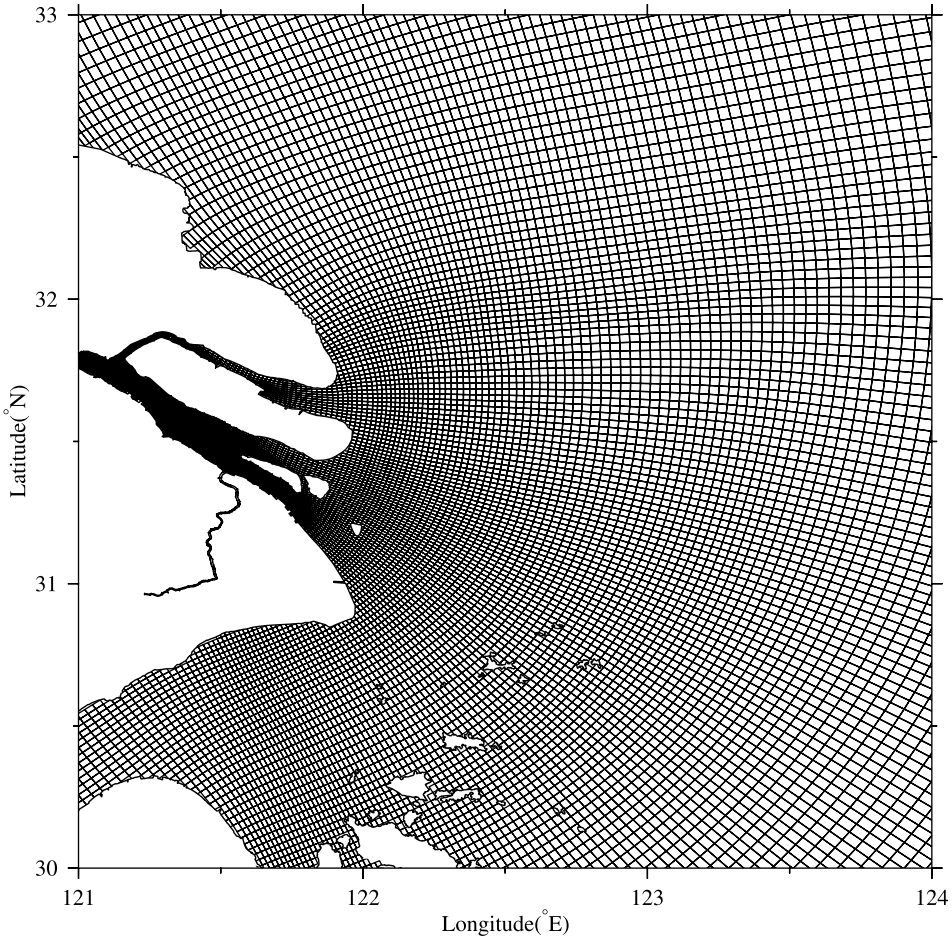

Figure 3. An enlarged view of the model mesh around the Changjiang River mouth.

(long-wave radiation), the evaporation heat flux, and the sensible heat flux.

2.2. Skill Assessment Methods

[13] Model results were evaluated against the observed data via the correlation coefficient (CC)

$$\mathrm{CC} = \frac{\sum_{i=1}^{N}(X_{\mathrm{mod}} - \bar{X}_{\mathrm{mod}})(X_{\mathrm{obs}} - \bar{X}_{\mathrm{obs}})}{\left[\sum_{i=1}^{N}(X_{\mathrm{mod}} - \bar{X}_{\mathrm{mod}})^2 \sum_{i=1}^{N}(X_{\mathrm{obs}} - \bar{X}_{\mathrm{obs}})^2\right]^{1/2}} \quad (3)$$

the root-mean-square error (RMSE)

$$\mathrm{RMSE} = \left[\sum_{i=1}^{N}(X_{\mathrm{mod}} - X_{\mathrm{obs}})^2/N\right]^{1/2} \quad (4)$$

and the skill score (SS) [*Allen et al.*, 2007; *Liu et al.*, 2009a; *Murphy*, 1988; *Ralston et al.*, 2010]:

$$\mathrm{SS} = 1 - \frac{\sum_{i=1}^{N}(X_{\mathrm{mod}} - X_{\mathrm{obs}})^2}{\sum_{i=1}^{N}(X_{\mathrm{obs}} - \bar{X}_{\mathrm{obs}})^2} \quad (5)$$

where X is the variable of interest and $\bar{X}$ is the time mean. Performance levels are categorized by *SS* as: >0.65 excellent; 0.65–0.5 very good; 0.5–0.2 good; <0.2 poor [*Maréchal*, 2004; *Allen et al.*, 2007; *Ralston et al.*, 2010].

[14] For the tide, we further used the vectorial difference suggested by *Foreman et al.* [1993]:

$$\mathrm{Diff} = \left[(a_o \cos g_o - a_m \cos g_m)^2 + (a_o \sin g_o - a_m \sin g_m)^2\right]^{1/2} \quad (6)$$

where (a_o, g_o) are the observed harmonic amplitude and phase, respectively; (a_m, g_m) are the modeled amplitude and phase, respectively. We also calculated the relative vectorial difference to standardize the error performance:

$$\mathrm{RDiff} = \mathrm{Diff}/a_o \quad (7)$$

2.3. Numerical Experiments Setting

[15] After validations, four experiments were conducted (i.e., Exp1 through Exp4) to investigate the physical mechanisms of the tidal modulation to the Changjiang River

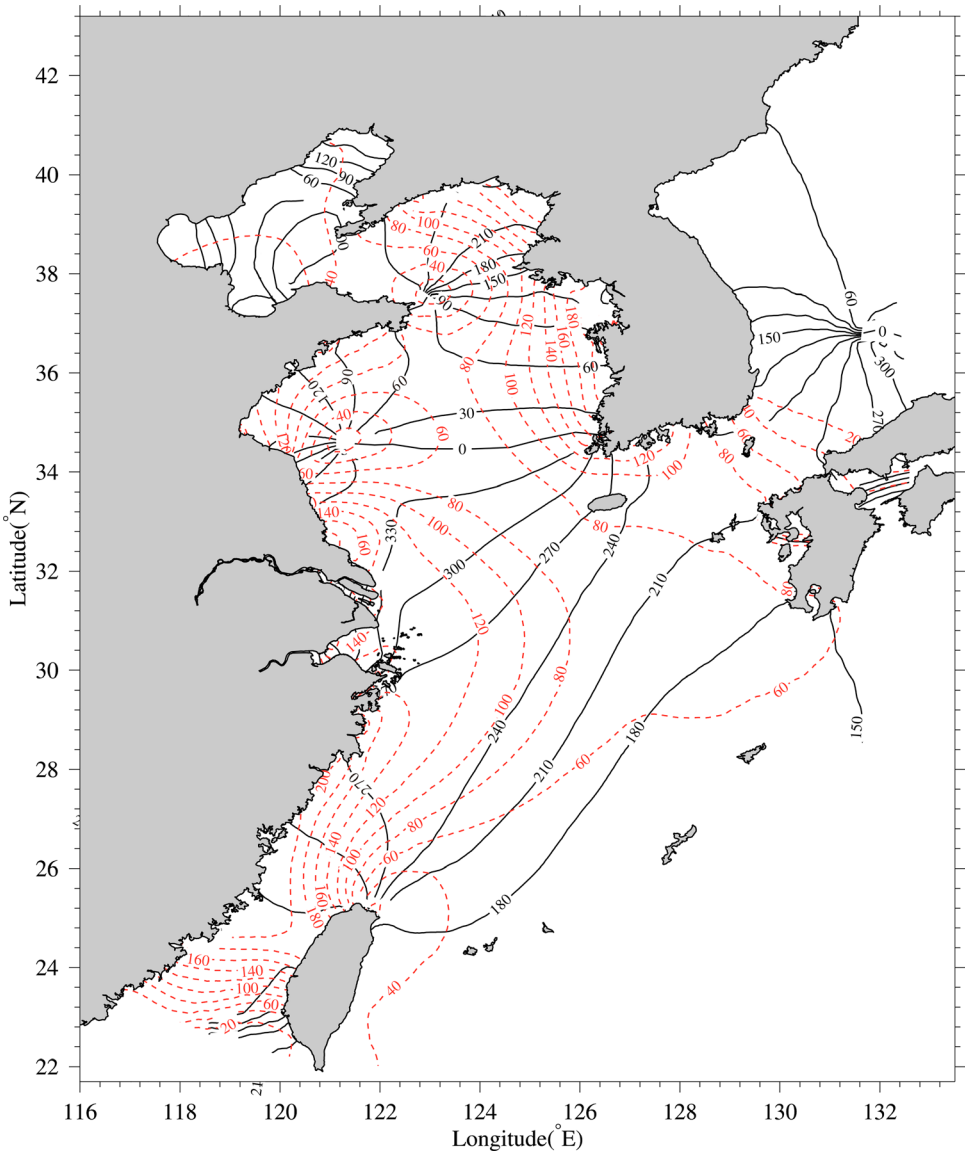

Figure 4. Cophase line (black solid lines, interval 30°) and coamplitude line (red dashed lines, interval 20 cm) of the M_2 tide constituent.

plume. In Exp1 we only considered the constant runoff of 50,000 m^3 s^{-1}, approximate the annually mean value in summer [*Shen et al.*, 2003]. Exp2 added the tidal forcing to Exp1. External forces such as wind, shelf currents, and surface heating were not included. Through analyzing the results from these two idealized experiments, we can understand the inherent property of tidal modulation for the Changjiang River plume. Exp3 added the external forcings to Exp1, i.e., the characteristic summer wind of 4 m s^{-1} southerly (via analyzing the *NCEP* wind), the shelf currents, and the surface heating, but without the tide. Exp4 added the tide onto Exp3. These two experiments aimed to further evaluate the tidal modulation under the external forcings. All the experiments ran from a cold start for 90 days. The results of the last 30 days were analyzed. We selected a tide-averaging window of 6 M_2 periods, or nearly 3 days, both during the spring and neap tides, which gives lower relative error [*Wu et al.*, 2010].

3. Model Validations

3.1. Validation of Harmonic Tide

[16] Tide in the YECS region is well known to have large amplitude and produce strong tidal currents [*Choi*, 1980]. Tide from the northwest Pacific propagates from the continental shelf and rotates in the Yellow Sea basin. A couple of tidal nodal points can be found in the Yellow Sea and Bohai Sea [*Choi*, 1980; *Editorial Board for Marine Atlas*, 1992]. Basically, the plume region is influenced by two tide systems: the propagating tide system in the East China Sea and the rotating tide system in the Yellow Sea [*Shen et al.*, 2003]. Our model successfully simulated such tide systems

Table 1. Correlation Coefficient (CC), Root-Mean-Square Error (RMSE), and Skill Score (SS) of Each Validation[a]

			Validation in November 2005				Salinity Validation in August 2008 (psu)			
	Tide Validation (m)		Tidal Current (m/s)		Salinity (psu)		Salinity (psu)		Without Tide	
	Total	Plume Region	Surface	Bottom	Surface	Bottom	Surface	Total	Surface	Total
CC	0.94	0.95	0.86	0.89	0.89	0.97	0.74	0.82	0.46	0.49
RMSE	0.29	0.27	0.38	0.19	3.97	3.01	6.64	3.88	10.14	6.55
SS	0.91	0.93	0.71	0.72	0.59	0.83	0.51	0.71	−0.14	0.16

[a]For the tidal validation (harmonic tide versus modeled tide), "total" represents all 14 stations, and "plume region" signifies the four selected stations (numbers 7, 8, 9, and 10). For the validation in August 2008, "total" represents the layers of surface, 5 m, 10 m, and 20 m. All the data of each category are pooled together to calculate the statistical assessments.

(Figure 4; for comparison refer to *Editorial Board for Marine Atlas* [1992]), except the two nodal points in the Bohai Sea, which may be restricted by the grid resolution in that area and is far away from the region we studied.

[17] The numerical model was validated at 14 tidal gauge stations around the Changjiang River mouth (for positions see Figures 1a and 1b). The total skill score at all 14 stations was 0.91 and that of the stations in the plume region (represented by Stations 7, 8, 9, and 13) was 0.93 (Table 1), excellent according to the classification by *Maréchal* [2004]. Correlation coefficient and RMSE were both reasonable. Comparison of harmonic constants and the associated vectorial differences of the 4 major constituents, M_2, S_2, K_1, and O_1, are shown in Table 2. In this region, M_2 is the strongest constituent followed by the S_2. The mean difference of M_2 was 0.14 m, accounting for 12.39% of the observed amplitude on average. The mean difference of S_2 was 0.09 m, while its mean relative difference was similar to that of M_2. Mean differences of K_1 and O_1 did not exceed 0.05 m. Overall, the model showed a reasonable skill. The relative differences were approximate the same level of many previous studies [e.g., *Tsimplis et al.*, 1995; *Xu et al.*, 2010].

3.2. Modeled Shelf Currents in Summer

[18] During the last several decades, a number of studies were conducted on the shelf currents in the YECS region and the researchers have reached a good consensus on their major patterns [e.g., *Nitani*, 1972; *Lü et al.*, 2006; *Ma et al.*, 2010]. Particularly, *Lü et al.* [2006] presented a sketch map of the shelf currents in this region (via their personal communication with Y. X. Tang in 2005) based on the analysis of the historical data of multifold sources from 1906 to 2003. Similar to most of the other previous studies, this sketch map characterizes a couple of parallel current systems roughly from the southwest to the northeast along the isobaths. The warm and strong western boundary current, Kuroshio, flows along the Ryukyu Trench. After leaving the Taiwan Strait, part of the TWC veers to the right and joins the Kuroshio and the remainder flows toward the Changjiang River mouth. In summer, the southerly wind drives significant East China Sea Coastal Current (ECSCC) that flows northward along the Chinese coast accompanying the TWC. East of the Changjiang River mouth, an eastward current can be identified that flows toward the Tsushima-Korea Strait, which carries the Changjiang Diluted Water (CDW).

[19] We ran our model under the summer climatological wind and the heating-related parameters from NCEP, the initial salinity and temperature distribution from SODA (Simple Ocean Data Assimilation), and the Changjiang runoff (50,000 $m^3 s^{-1}$) from the data observed by the Changjiang Water Resource Commission. After spun up for 60 days,

Table 2. Comparison Between the Modeled and Observed Amplitude (A in m) and Phase (θ in deg) of the Four Major Tide Constituents of M2, S2, K1, and O1[a]

		M2(A/θ)[b]				S2(A/θ)[c]				K1(A/θ)[d]				O1(A/θ)[e]			
Number	Station	Mod	Obs	Diff	RDiff(%)	Mod	Obs	Diff	RDiff(%)	Mod	Obs	Diff	RDiff(%)	Mod	Obs	Diff	RDiff(%)
1	Haimen	1.67/267	1.56/270	0.14	8.9	0.84/325	0.91/330	0.1	11.4	0.35/226	0.30/243	0.11	36	0.27/173	0.18/197	0.13	71.4
2	Xize	1.39/268	1.36/264	0.1	7.4	0.75/323	0.83/318	0.11	12.7	0.32/220	0.28/227	0.05	19.4	0.24/167	0.23/171	0.02	8.4
3	Shenjiamen	1.22/274	1.12/267	0.17	15.6	0.68/323	0.62/320	0.07	11.1	0.30/217	0.26/225	0.06	21.5	0.24/164	0.23/162	0.01	5.6
4	Dinghai	0.93/294	0.85/287	0.13	15.9	0.51/352	0.46/344	0.08	18.3	0.31/225	0.25/219	0.07	26.7	0.23/173	0.21/175	0.02	10.2
5	Daishan	1.13//302	0.91/293	0.27	29.8	0.55/345	0.50/348	0.06	11.4	0.32/212	0.25/219	0.08	31.2	0.22/166	0.21/173	0.03	13.4
6	Tanhu	1.39/355	1.43/349	0.15	10.7	0.79/59	0.85/51	0.13	15.2	0.26/240	0.24/237	0.02	10	0.20/189	0.21/182	0.03	12.8
7	Lvhuashan	1.24/291	1.13/284	0.18	16.1	0.66/338	0.74/332	0.11	15.0	0.29/204	0.31/202	0.02	7.6	0.20/152	0.23/155	0.03	15.8
8	Luchaogang	1.43/331	1.45/329	0.05	3.7	0.84/33	0.89/26	0.12	13.1	0.27/230	0.25/225	0.03	12.1	0.19/169	0.21/164	0.03	12.6
9	Zhongjun	1.12/332	1.13/329	0.06	5.3	0.69/34	0.75/29	0.09	11.6	0.20/215	0.24/218	0.04	17.3	0.15/169	0.17/168	0.02	11.9
10	Lvsi	1.54/352	1.61/350	0.09	5.5	0.90/53	0.97/43	0.18	18.3	0.11/144	0.12/151	0.02	14.4	0.06/100	0.10/103	0.04	40.2
11	Binhaigang	0.67/227	0.84/222	0.18	21.7	0.35/317	0.30/307	0.08	25.1	0.21/25	0.28/20	0.07	26.1	0.14/337	0.20/342	0.06	30.9
12	Lianyungang	1.55/171	1.63/179	0.24	14.5	0.72/241	0.70/242	0.02	3.4	0.27/13	0.25/13	0.02	8	0.18/316	0.20/321	0.03	13
13	Rizhaogang	1.38/156	1.42/160	0.11	7.4	0.64/226	0.59/222	0.07	11.2	0.25/6	0.24/0	0.03	11.5	0.18/305	0.20/312	0.03	15.3
14	Qingdao	1.17/125	1.26/130	0.14	11	0.56/188	0.53/192	0.05	9.1	0.24/352	0.23/3	0.05	20.1	0.16/291	0.19/300	0.04	21.4

[a]Mod, modeled; Obs, observed; Diff, the vectorial difference; RDiff, the relative vectorial difference that is normalized by the observed amplitude.
[b]Mean: Diff, 0.14, RDiff, 12.39.
[c]Mean: Diff, 0.09, RDiff, 13.35.
[d]Mean: Diff, 0.05, RDiff, 18.7.
[e]Mean: Diff, 0.04, RDiff, 20.20.

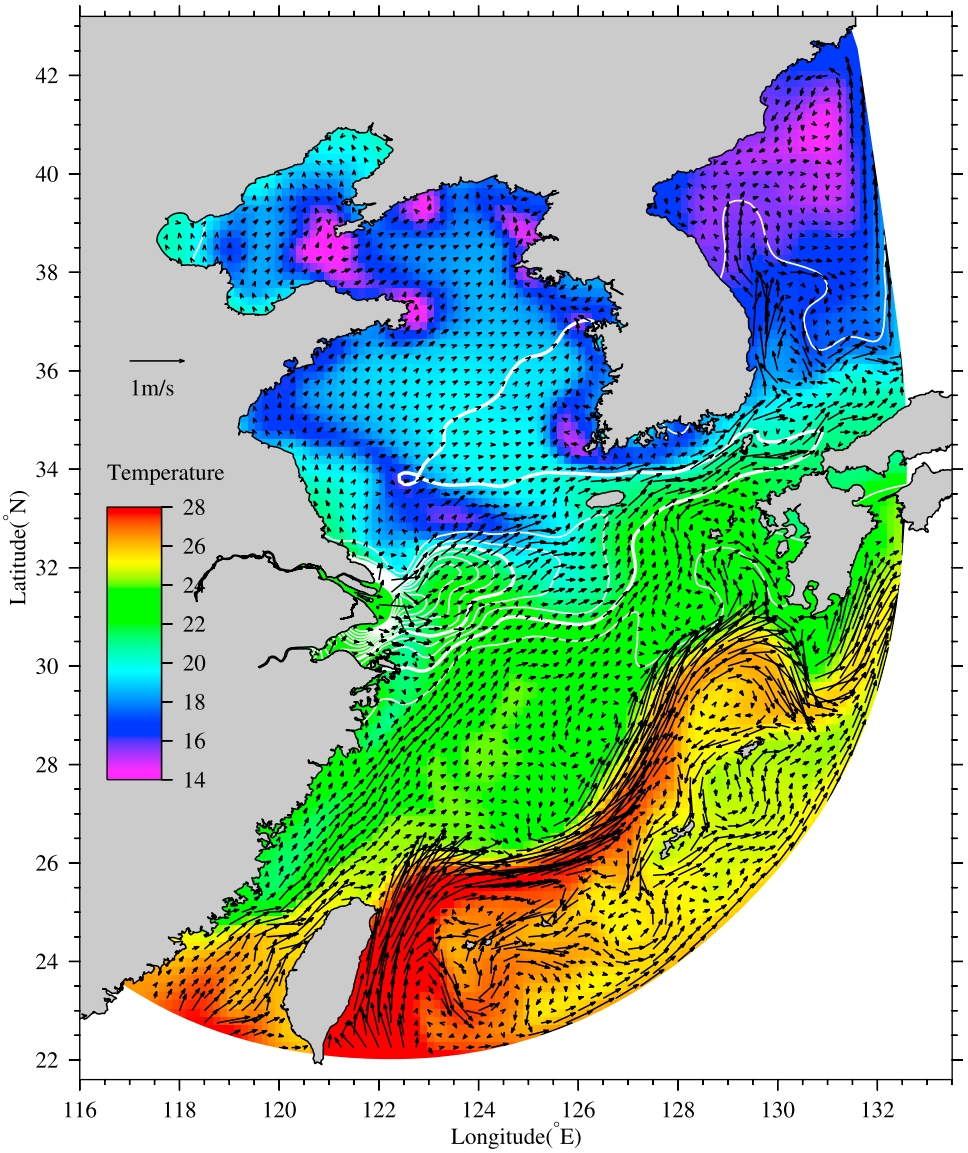

Figure 5. Modeled tidal-averaged (during the spring tide) surface currents, temperature (color scale), and salinity (white contours, interval of 2 psu) under the summer climatological conditions. To better visualize, current vectors were selected every 1/4°. The isohalines 26 and 32, which are often treated as the boundaries of the Changjiang diluted water, are signified by thick lines.

the modeled surface currents, temperatures, and salinity were output and their tidally averaged values are shown in Figure 5. It can be seen that almost all the shelf currents were well characterized and were consistent with the sketch map of *Lü et al.* [2006].

3.3. Validations of the Tidal Current and Salinity in November 2005

[20] Salinity and current observations obtained from 12 shipboard stations around the plume region (for locations, see Figure 1b) by the State Key Laboratory of Estuarine and Coastal Research (SKLEC) during early November 2005 were used for validation. Six small fishing ships were used and each was in charge of 2 stations. Each station lasted for at least 26 h and the tidal salinity and current were obtained. More details of this survey can be seen in work by *Gao* et al. [2009]. Our model simulation began 1 May. After running for half a year with the observed runoff (Changjiang Water Resource Commission) and 6-hourly QSCAT/NCEP reanalyzed wind, the model results were output for comparison.

[21] Statistical assessments are shown in Table 1. Skill score of the modeled tidal current at all the stations (via the east and north components) is 0.71 at the surface and 0.72 at the bottom. RMSE is less than 0.4 m s^{-1}. Considering the maximum velocity exceeds 2.0 m s^{-1} at SH2, SH5, ZJ1, and ZJ2, such an error is acceptable. The correlation coefficient is high as expected, because the tide dominates the currents in this region.

[22] Figure 6 shows the modeled salinity and observations. The tidal variations and surface-bottom differences were

well reproduced. The model showed a reasonable skill score of 0.59 at the surface and an excellent skill score of 0.83 at the bottom. The relatively lower skill of the surface salinity may result from the rapid response of the plume to the changing wind [*Liu et al.*, 2009b]. The correlation coefficient is high for both surface and bottom. Considering that the observation stations roughly covered a large portion of the plume region, the high correlation coefficient suggests that the numerical model well captured the plume pattern both for the spatial distribution and for the temporal variation.

3.4. Validation of the Cruising Survey Data Observed During August 2008

[23] During 11 and 13 August 2008, SKLEC conducted a cruising survey by using three small vessels. Sampling sites are shown in Figure 1b. Each vessel surveyed two latitudinal sections. Because the observations were not synoptic, we compared the modeled salinity at the exact time when each data measurement was obtained. To better visualize the validation results, we grouped the sampling sites as shown in Figure 1b.

[24] The model ran from 1 May 2008, and was driven by the observed Changjiang runoff and the QSCAT/NCEP reanalyzed wind. Figure 7 shows the comparisons of the model results against the observed data at the surface and 5 m, 10 m, and 20 m depths. Overall, the model fairly well reproduced the salinity at 5 m, 10 m, and 20 m. Modeled surface salinity was underestimated in the northern portion of the plume but was overestimated in its eastern portion. The skill score was 0.51 at the surface (Table 1), acceptable given the high variability of surface plume and the criteria of *Maréchal* [2004]. The skill score was 0.73 for the entire water column. Correlation coefficients were reasonable both for the surface and the entire water column, indicating that the model captured the plume pattern quite well. RMSE was somewhat larger than expected, probably due to the rapidly changing tide and wind that provided a big challenge to the numerical simulation.

[25] An identical run without the tide was conducted, and the results are shown by the gray dots in Figure 7 and the associated skills are listed in Table 1. Significant error appeared. The nontidal experiment showed a small or even negative skill score, great RMSE, and small correlation coefficient. Hence, the plume patterns were incorrect. This experiment highlighted the importance of tide in correctly simulating a river plume.

3.5. Modeled Climatological Salinity Distribution in Summer

[26] We compared the modeled Changjiang River plume against the summer climatological plume pattern that was documented by the *Editorial Board for Marine Atlas* [1992]. Model settings were the same as section 3.2. An additional run without tide was also conducted. The experiments ran 60 days initially for spin up, and the results from an additional 30 days were tidally averaged for comparison.

[27] Figure 8a is the summer surface salinity distribution digitized from the marine atlas [*Editorial Board for Marine Atlas*, 1992]. After leaving the river mouth, the Changjiang River plume turns to the northeast toward Jeju Island. Because of the great variability of the wind and runoff under the real-time conditions, we do not expect the modeled result to match the climatological sketch map exactly. However, the model result was fairly reasonable (Figure 8b). Both the plume extension direction and the frontal width were consistent with the climatological pattern. If we examine a model run excluding the tide as shown in Figure 8c, the model result showed a very different distribution. A strong northward extension appeared. The diluted water mass covered a much larger area than the climatological distribution and the modeled result with the tidal forcing. The associated physical mechanisms will be discussed in section 4.

4. Results and Discussion

4.1. Tidal Modulation Under the Windless Condition and Without the Shelf Currents

[28] It is natural and useful for the first step to exclude the external forcings such as the wind and shelf currents, but only retain the runoff and tide (Exp1 and Exp2), to explore the inherent property of the tidal modulation on the Changjiang River plume.

4.1.1. Changjiang River Plume Without the Tide

[29] If only considering the runoff (no tide, wind and shelf currents, i.e., the Exp1), a large portion of the Changjiang diluted water spread northwestward along the Jiangsu coast after leaving the river mouth (Figure 9a), which showed a similar pattern as Figure 8c did. This was opposite to the propagation of a coastally trapped wave, referred to upstream extension hereafter. Downstream flow was formed at the seaward edge of the plume, where a train of baroclinic waves or eddies occurred that was similar to the previous simulation by *Chen et al.* [2008]. Overall, without the tidal forcing, the Changjiang River plume featured an expected anticyclonic rotation [*Chao*, 1988; *Yankovsky and Chapman*, 1997], but was dramatically elongated and extended to the upstream.

[30] An upstream extended buoyant river plume like that shown in Figure 9a seems to conflict with the effect of Coriolis force, but similar results occurred frequently in numerical simulations under the specifications like those of Exp1 (i.e., without tide, wind, nor ambient currents), and were observed in several regions (a detailed literatures review can be found in work by *Matano and Palma* [2010]). *Woods and Beardsley* [1988] deduced that under the high river discharge events, due to the increased depth offshore, the positive vorticity will be produced due to the potential vorticity conservation, which tends to push the fresh plume to the upstream. *Matano and Palma* [2010] addressed that the upstream plume extension is associated with the geostrophic adjustment of the buoyant discharge, which creates an onshore baroclinic gradient force that drives a diversion of the discharge in the upstream direction.

[31] Based on these previous studies, the plume extension from Exp1 is not surprising, and similar patterns can also be found in several other numerical studies of the Changjiang River plume that excluded the tide. Because many plumes in the well-sampled regions extend to the downstream, as *Matano and Palma* [2010] concluded, it is a common practice in numerical studies to add a downstream mean flow solely to arrest the upstream development [*Yankovsky and Chapman* 1997; *Fong and Geyer* 2002; *Narayanan and Garvine* 2002; *Guo and Valle-Levinson* 2007]. The problem is, although in some areas the downstream background current is supported by the field data (e.g., out of the Chesapeake Bay [*Epifanio*

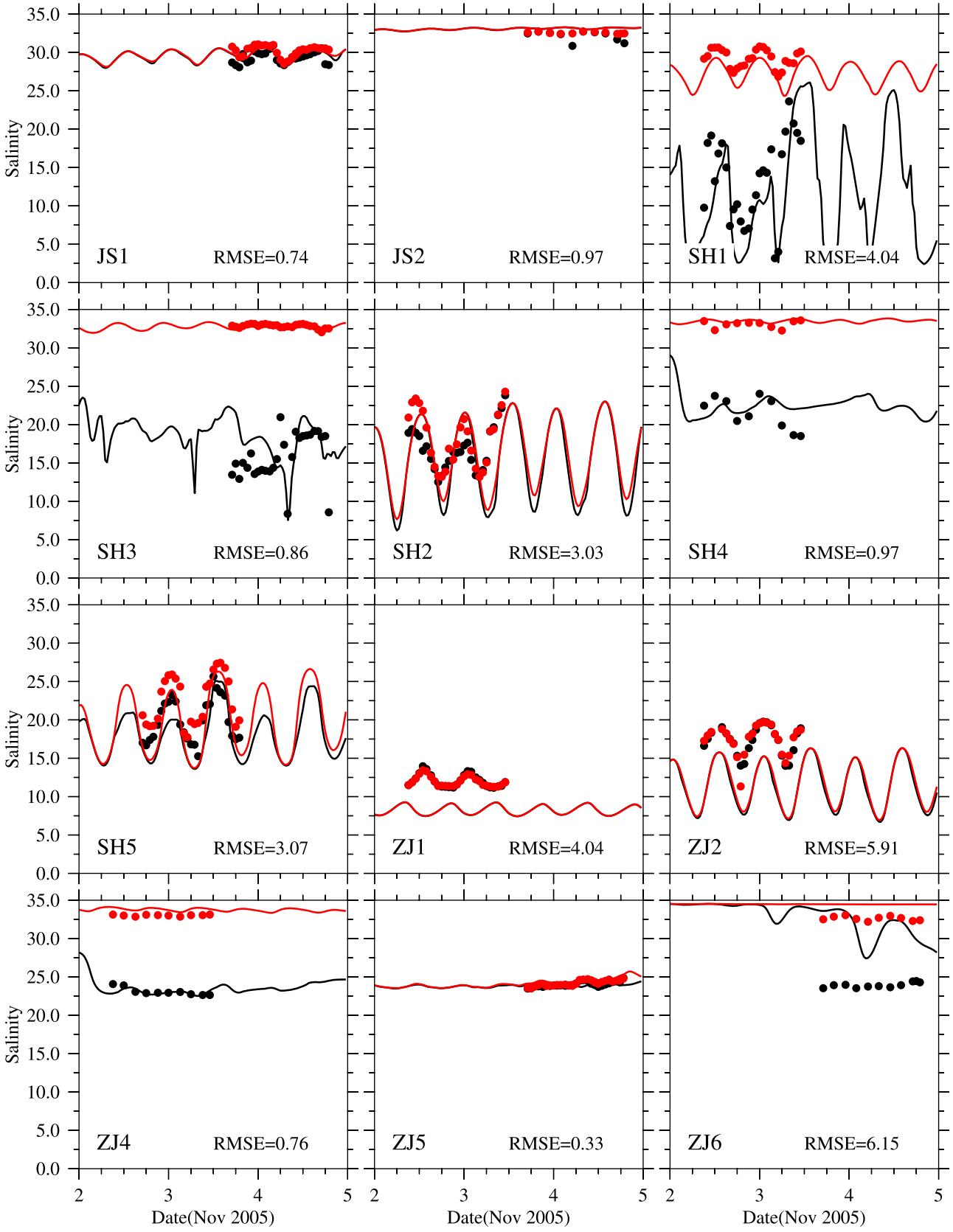

Figure 6. Validations of the surface (black) and bottom (red) salinity during November 2005. Dots signify the observed data; lines represent the model results. For station locations, see Figure 1b. The RMSE value at each station is labeled.

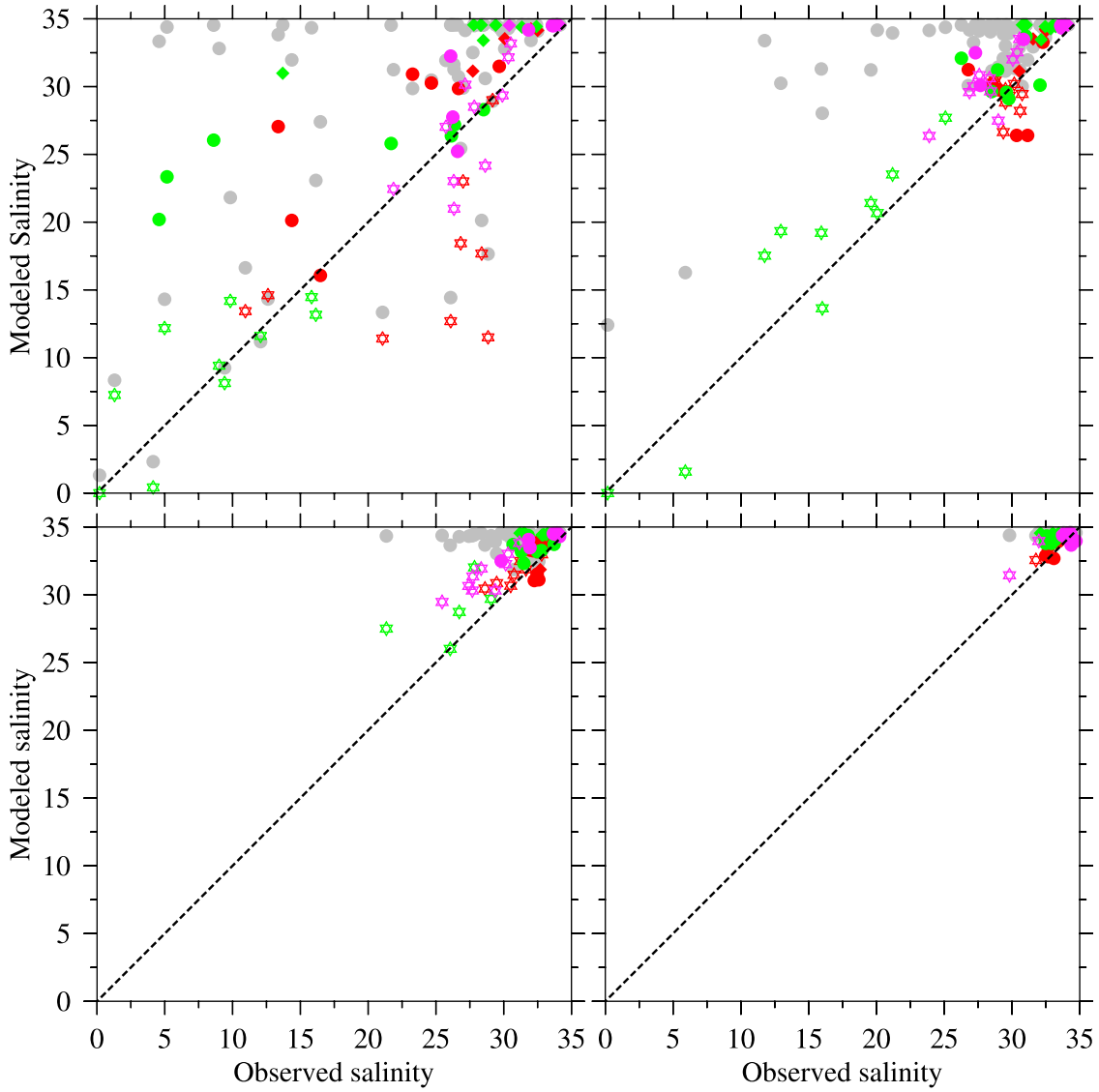

Figure 7. Salinity validations in August 2008 at the surface, 5 m, 10 m, and 20 m. For the meanings of the symbols see Figure 1b. The gray dots signify the results from the nontidal run.

and Garvine, 2001]), many others are not. For the case of the Changjiang River plume, such an upstream extension was rarely observed. Also there is no prevailing downstream ambient current near the coast. Although occasionally there exists a southward current offshore the Jiangsu coast [e.g., *Lü et al.*, 2006], its location is too remote to influences the plume extension in the coastal region.

4.1.2. Influence of the Tide in Arresting the Upstream Extension

[32] When we added the tidal forcing (i.e., as in the Exp2), the upstream extension vanished (Figure 9b). Instead of generating any downstream background current, the tide can produce an upstream residual current along the Jiangsu coast due to its nonlinear interaction with the shallow topography as reported by *Wu et al.* [2010]. This implies that the tidal mixing rather than the tidal nonlinearity arrests the upstream extension.

[33] Sectional profiles of salinity and turbulent viscosity were plotted with and without the tide (Figure 10). Without the tidal forcing, the turbulent viscosity was small (Figure 10c) and, therefore, high stratification occur near the surface (Figure 10a). With the tidal forcing, strong turbulent mixing occurred in the middle and lower layers (Figure 10d), and the water column became well mixed (Figure 10b). According to the study by *Chen and Beardsley* [1995], the vertical mixed bottom layer thickness h_m can be estimated as

$$h_m = \left(\frac{16\gamma\delta\Delta T U^3}{N^2\pi}\right)^{1/3} \tag{8}$$

where γ is the bottom friction coefficient, usually taken as 2.5×10^{-3}; δ is the efficiency of tidal kinetic energy dissipation used over the period ΔT to produce the potential energy needed for the vertical mixing and was suggested to be 3.7×10^{-7} by *Simpson and Hunter* [1974]. U is the tidal velocity and was set to 1 m/s as a typical value in this region. N is the Brunt-Väisälä frequency. ΔT was suggested to be 10 days under the weak stratification condition and 14 days

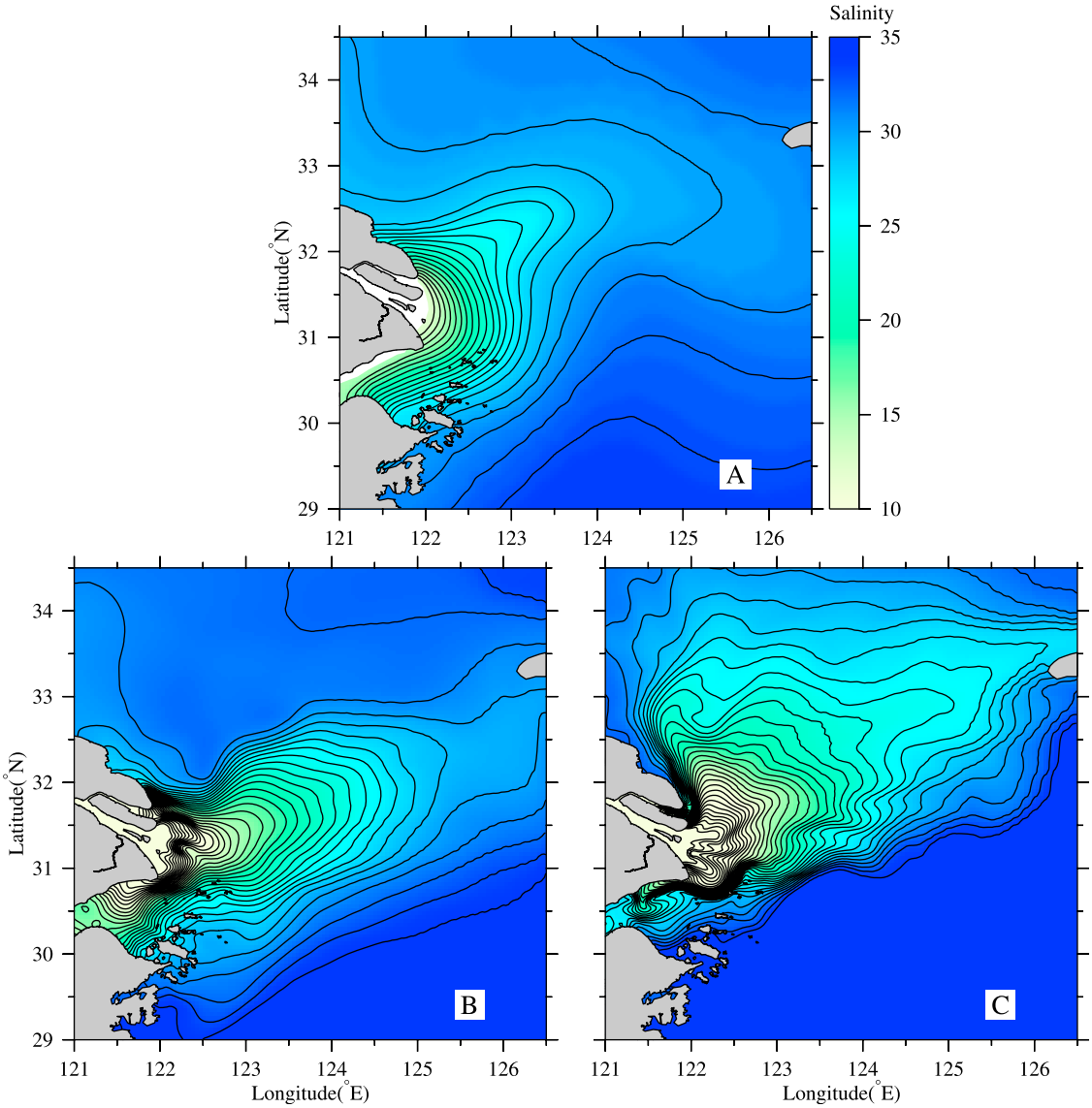

Figure 8. (a) Summer climatological surface salinity distribution from the marine atlas [*Editorial Board for Marine Atlas*, 1992]. (b) Modeled monthly averaged salinity in summer under the climatological conditions with tide. (c) Modeled salinity in summer under the climatological conditions without tide.

in the strong stratification case in the Yellow Sea [*Lee and Beardsley*, 1999]. To restrict the bottom mixed layer below the surface, i.e., $h_m < 10$, the required N^2 should at least be 0.057. While Figure 10a indicates the N^2 in the nontidal case was only about 0.015. The tide along the Jiangsu coast was strong enough to mix the water column, as indicated by Figure 10b.

[34] A strong along-coastal baroclinic gradient was thereby formed at the northern side of the Changjiang River mouth, which drove a cross-coastal flow and prevented the upstream extension of the plume (Figure 9). A similar mechanism was found in the model study of the Chesapeake Bay plume [*Guo and Valle-Levinson*, 2007]. Because the tide exists at most regions of the world, this may give an additional explanation as to why most river plumes turn to the downstream direction besides the Coriolis forcing.

4.1.3. Tide-Forced Plume Pattern and Its Spring-Neap Variation

[35] Besides arresting the upstream plume extension, the tidal forcing also modulated the Changjiang River plume into distinguishable spatial structures with significant spring-neap variation. During the spring tide the Changjiang River plume turned to the downstream at first inside the 30 m isobath (Figure 9b, a zoom-in view was shown in Figure 9d). We refer this portion of plume portion as the near-field plume, following the definition by *MacCready et al.* [2009]. A great portion of the plume turned to the northeast at approximate 122.5°E, and then it rotated anticyclonically to the downstream. A significant bulge occurred around the head of submarine canyon. Previous study by *Yankovsky and Chapman* [1997] suggested that, under intermediate conditions of depth and river flow velocity, a plume will turn downstream at first

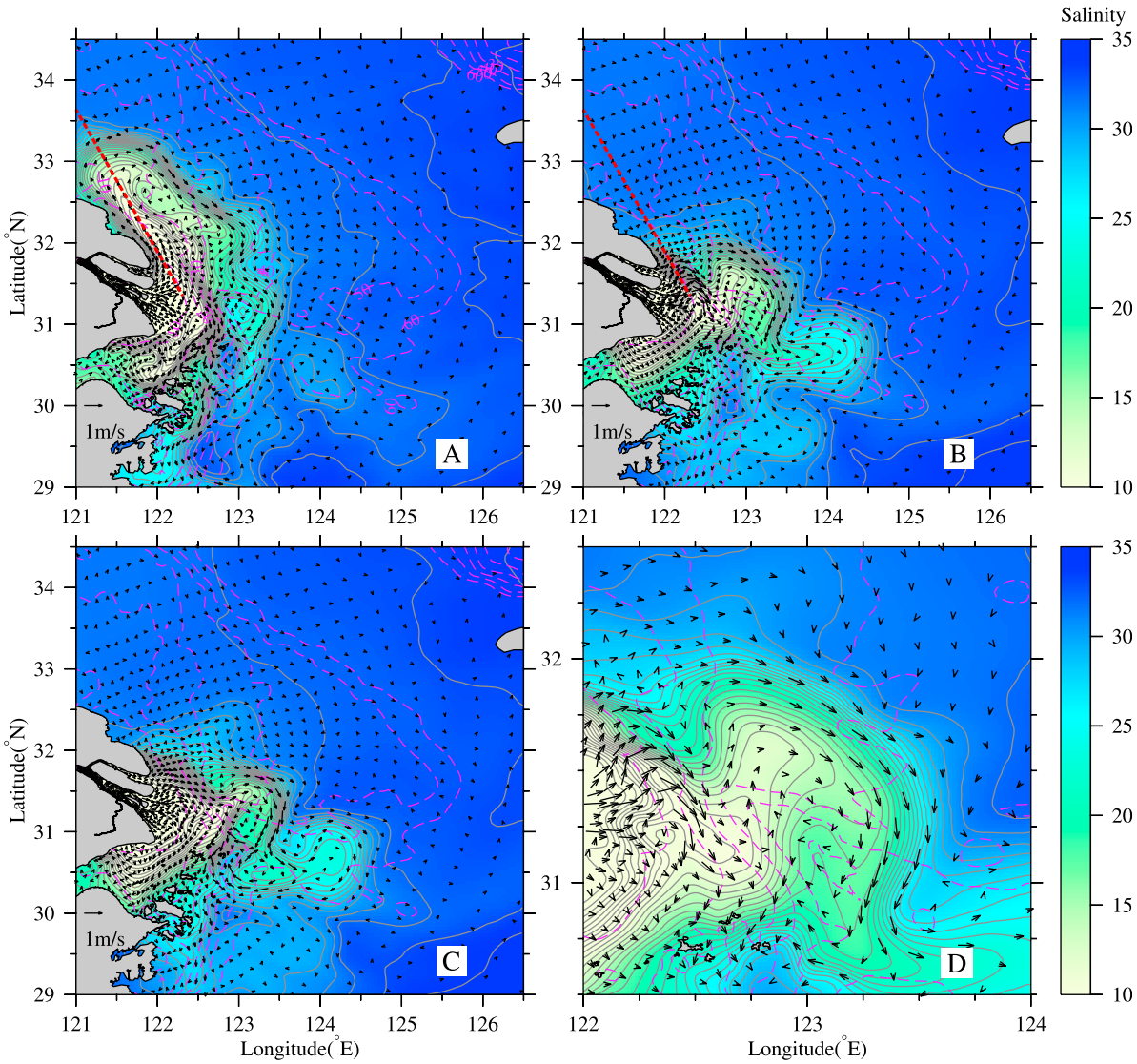

Figure 9. (a) Modeled surface salinity and current distributions from Exp1. Purple dashed lines are the isobaths. Red dashed line is the location for sectional profile in Figure 10. (b) Tidal-averaged surface salinity and residual currents during the spring tide from Exp2. (c) Tidal-averaged surface salinity and residual current during the neap tide from Exp2. (d) A zoom-in view of Figure 9b around the submarine canyon.

as a bottom-trapped plume and will then rotate anticyclonically to form a bulge as a surface-trapped plume. *Ge et al.* [2008] also described such a mechanism of the Changjiang River plume. The pattern shown in Figure 9b is fairly consistent with the results from these previous studies.

[36] However, such a bulge was weakened during the neap tide (Figure 9c), which implied that strength of the tide probably impacted on the bulge. In a previous study, we found that there is an anticyclonic tidal residual current at the head of the submarine canyon [*Wu et al.*, 2010, Figure 8]. The funnel-shaped canyon produced a local high of surface water level, especially during the spring tide (Figure 11a). Such a local high can drive an anticyclonic geostrophic residual under the adjustment of Coriolis force and produce a bulge of the diluted water (Figure 9b). During the neap tide, due to the reduced tidal energy, the local high was less evident and therefore the residual rotation became weak (Figure 11b). The mechanism driving the local high at the head of the submarine canyon was unclear. We speculated that it may have resulted from the tidal asymmetry due to the funnel-shaped canyon topography. During the flood tide, a large amount of water mass was converged by the canyon that increased the water level significantly. During the ebb tide, the flow around the canyon was relatively dispersive. Hence, the water level around the head of the canyon was relatively higher after tidal averaging. A similar anticyclone was found at the head of Hudson Valley off the Hudson River mouth [*Zhang et al.*, 2009]. Filling the submarine canyon can greatly weaken the anticyclonic bulge both off the Hudson [*Zhang et al.*, 2009] and Changjiang River mouths (not shown). Such an anticyclone off the Hudson River mouth exists regardless of the tidal forcing [*Zhang et al.*, 2009], but for the

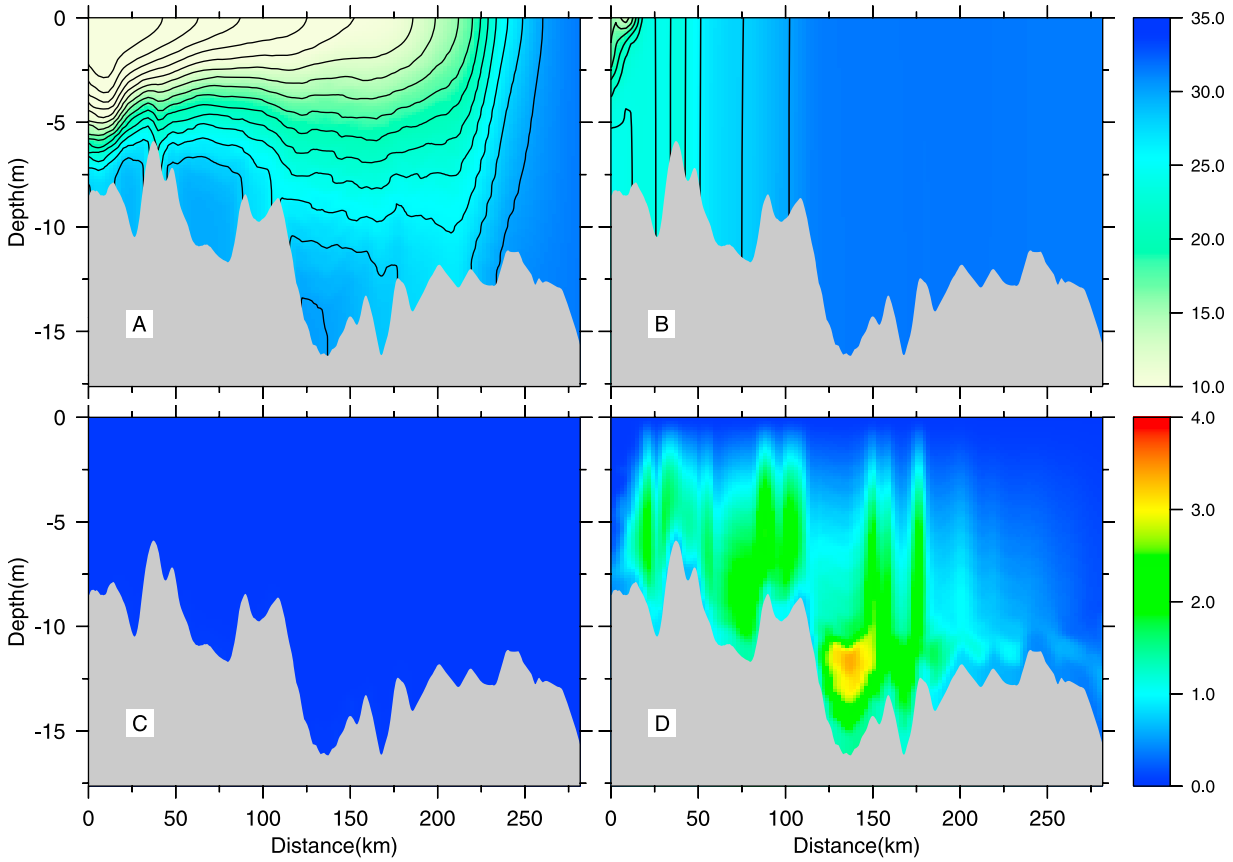

Figure 10. (a, b) Sectional salinity and (c, d) vertical turbulent viscosity (in units of 10^{-2} m^2 s^{-1}) from Exp1 (Figures 10a and 10c) and Exp2 (Figures 10b and 10d). For section position see Figure 9.

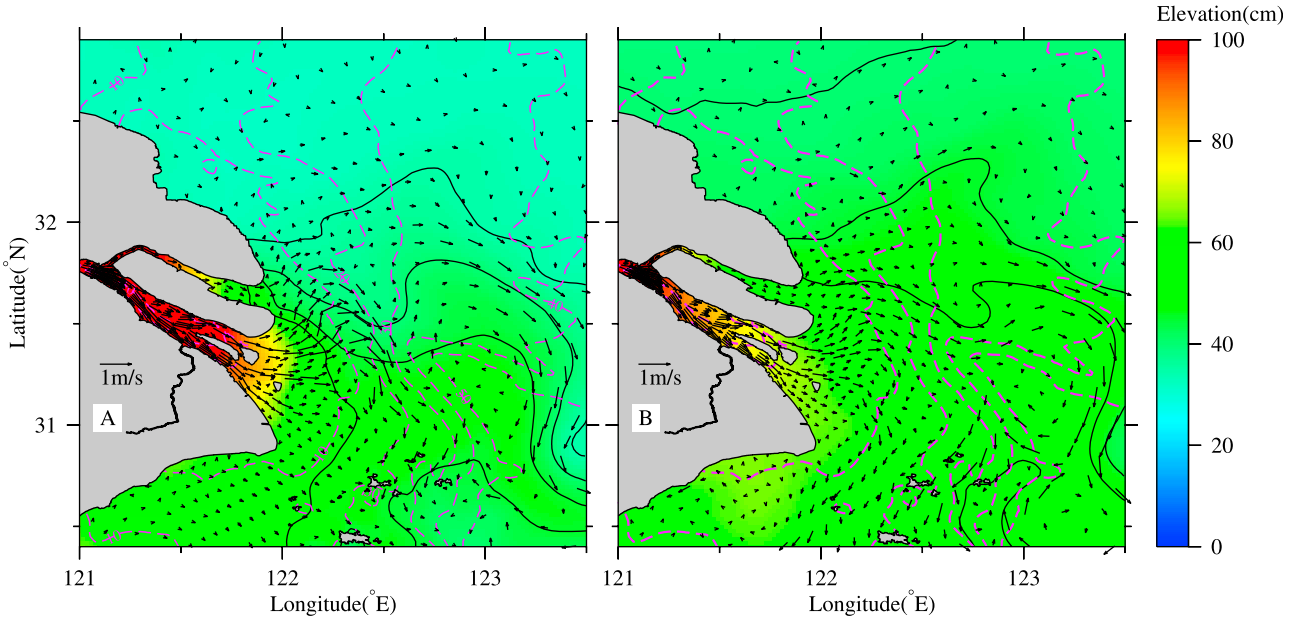

Figure 11. Tidal-averaged elevations during (a) the spring tide and (b) the neap tide from Exp2. Overlaid are the residual velocity and isobaths.

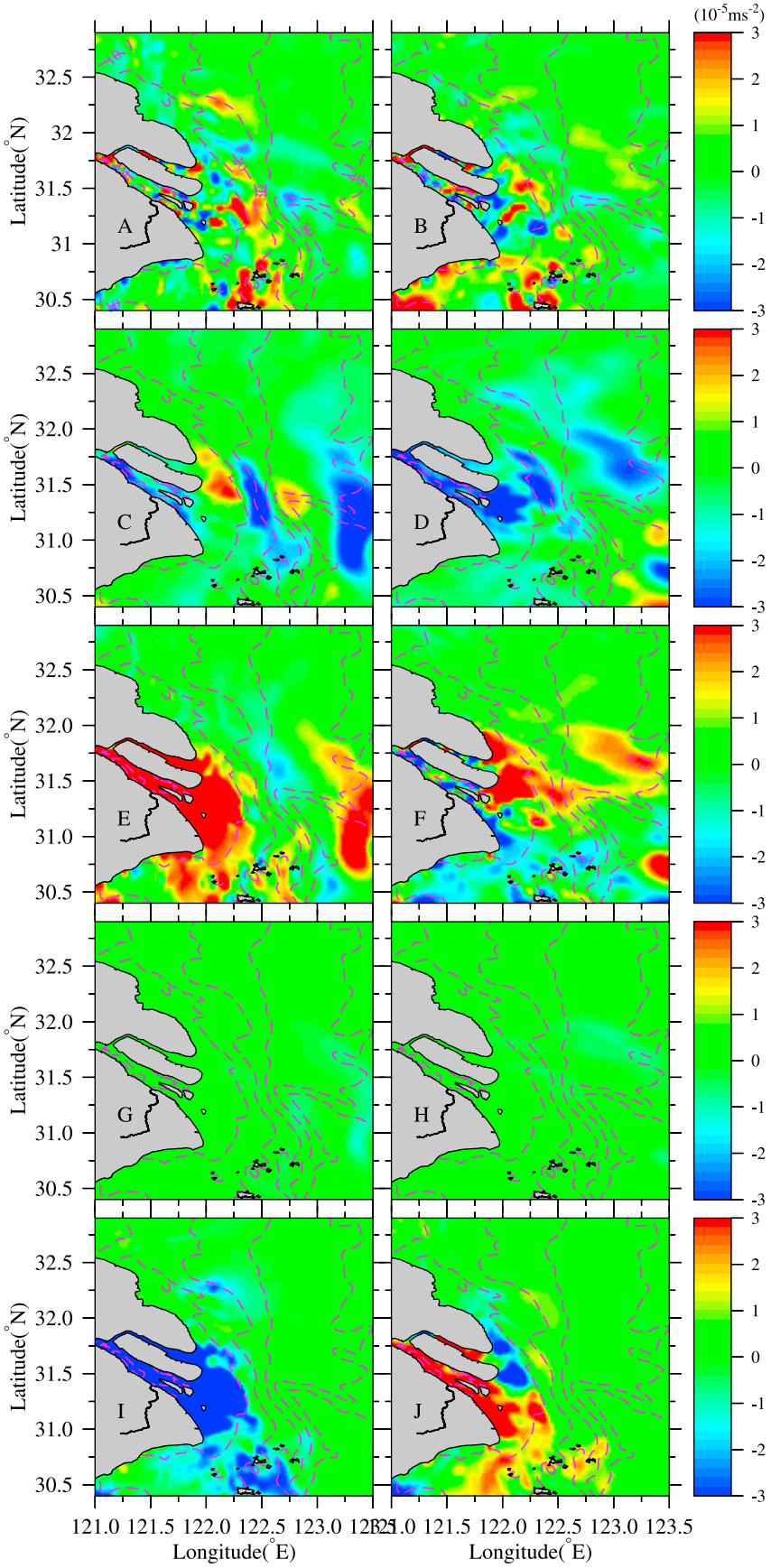
(10^-5 ms^-2)
A
B
C
D
E
F
G
H
I
J
Latitude(°N)
Longitude(°E)
121.0 121.5 122.0 122.5 123.0 123.5
30.5 31.0 31.5 32.0 32.5
-3 -2 -1 0 1 2 3

Figure 12

Changjiang River plume this structure vanishes when excluding the tide (Figure 9a) or becomes weakened during the neap tide (Figure 9c).

[37] Interestingly, because of the rotation of the bulge, a northeastward freshwater tongue occurred near 122. 5°E (during the spring tide, Figure 9d) or 123°E (during the neap tide, Figure 9c), which is a phenomenon frequently reported in summer and is often attributed to the southerly wind and shelf currents [*Chang and Isobe*, 2003; *Zhao*, 1991; *Zhou et al.*, 2009; *Zhu et al.*, 1997]. Note the wind forcing and the shelf currents were not included in Exp2. This indicated that the northeastward extension is an inherent feature of the Changjiang River plume. After rotating around the bulge, the diluted water flowed southward and merged into the far field plume as expected (Figures 9b and 9c), where the plume was thin, unstable, and can be easily disturbed by an external forcing such as the wind.

[38] Besides the bulge, a bidirectional structure is evident (Figure 9d). Before forming an anticyclone budge, a part of diluted water turned toward southeast. The separation was located near the head of the submarine canyon. This bidirectional structure was caused by tidal rectification and will be more pronounced with certain wind forcing, which will be further discussed. However, during the neap tide such a bidirectional structure became less evident (Figure 9c).

4.1.4. Tidal-Averaged Momentum Balance

[39] To further investigate the dynamic mechanisms that control the plume movement under the tidal forcing, the momentum balance in the upper 6 σ layers was analyzed. Averaged over 6 M_2 tidal cycles, the momentum balance was established as

$$0 = -\langle \vec{V} \cdot \nabla \vec{V} \rangle - f\vec{k} \times \langle \vec{V} \rangle - g\nabla_z \langle \zeta \rangle + \langle P_\rho \rangle + \left\langle \frac{\partial}{\partial z} Km \frac{\partial \vec{V}}{\partial z} \right\rangle \tag{9}$$

[40] All the terms of the momentum equation were moved to the right-hand side. Momentums in (9) are (in sequence) advection, Coriolis force, barotropic gradient force, baroclinic gradient force, and friction, respectively. The baroclinic force was small because we only consider the surface layers.

[41] During the spring tide, the momentum was balanced by advection, Coriolis force, barotropic gradient force, and friction inside the 10 m isobath (Figure 12). On the slope between the 10 m and 30 m isobaths, i.e., the frontal portion of the near-field plume, the momentum balance was mainly between the advection and the Coriolis force. Such a balance caused an along-isobath residual current, as shown in Figure 9d. This mechanism was previously recognized as the tidal rectification by *Loder* [1980]. With the cross-isobath-propagated tide acting on the slope, the rectified residual current is produced flowing along the isobath to the left (looking onshore). *Chen and Beardsley* [1995] reported that the rectified residual reaches its maximum at the surface and the momentum is balanced by advection and Coriolis force when the water column is homogenous. Conversely, when the water column is stratified, the momentum balance is more complicated and the rectified residual is a maximum at the subsurface along the tidal density front. However, by analyzing the vertical distribution of rectified residual current, we found that, although the slope region between the 10 m and 30 m isobaths is influenced by the stratified water, the maximum rectified residual current occurs at the surface. This is due to shallow water depth and strong tidal mixing off the Changjiang River mouth, which are different from the setting of *Chen and Beardsley* [1995].

[42] The funnel-shaped submarine canyon favored a tidally averaged surface water level setup at its head (Figure 11). Such a setup produced a barotropic gradient force (Figure 12f). Far away from the slope region, the plume was under a balance between the barotropic gradient force and Coriolis force, which produced a geostrophic flow.

[43] Because of the reduced tidal energy, during neap tide the momentum advection, as well as the tidal rectification, became small (Figure 13). Therefore the anticyclonic rotation of the near-field plume became weak (Figure 9c). Exterior to the 10 m isobath, the momentum balance was mainly established between the northward barotropic gradient force and the southward Coriolis force (Figure 13), and the freshwater flowed more seaward and the "bulge" became less evident (Figure 9c).

[44] It should be noted that the settings of Exp1 and Exp2 were quite idealized, because they excluded the wind forcing and shelf currents. It is important to know that to what degree the above plume characteristics are maintained under additional external forcings like the wind and shelf currents.

4.2. Tidal Modulation Under Southerly Wind and Shelf Currents

4.2.1. Plume Structure

[45] Superimposing the southerly wind of 4 m s^{-1} and the shelf currents, both the model runs with and without the tide showed a northeastward extension of the Changjiang River plume (Figure 14). However, significant differences can also be found between the results from these runs. Without tide, the plume also extended northward strongly as the mechanisms described above, and the diluted area was larger than the case with tidal forcing. By comparing to the windless scenarios (Figure 9), it is clear that the southerly wind, as well as the shelf currents, ultimately determines the northeastward extension of the Changjiang River plume. Nevertheless, in the region near the river mouth, the plume pattern still featured many similarities to the plume without wind. Particularly, the near-field plume and the bidirectional plume structure were maintained and were even more evident.

[46] During the spring tide, the near-field plume (Figure 14b, a zoom-in view was shown in Figure 14d) was similar to that of Exp2 (Figure 9d). The bulge merged into the far-field plume because of the wind-induced mixing and the northeastward Ekman transport. Most portions of the Changjiang River plume turned to the northeast at 122.5°E (Figure 14d), almost the same place as where the bulge originated in Exp2.

Figure 12. Tidal-averaged surface momentums in (a, c, e, g, i) x direction and (b, d, f, h, j) y direction during the spring tide from Exp 2. Shown are momentum advection (Figures 12a and 12b), Coriolis force (Figures 12c and 12d), barotropic gradient force (Figures 12e and 12f), baroclinic gradient force (Figures 12g and 12h), and friction (Figures 12i and 12j).

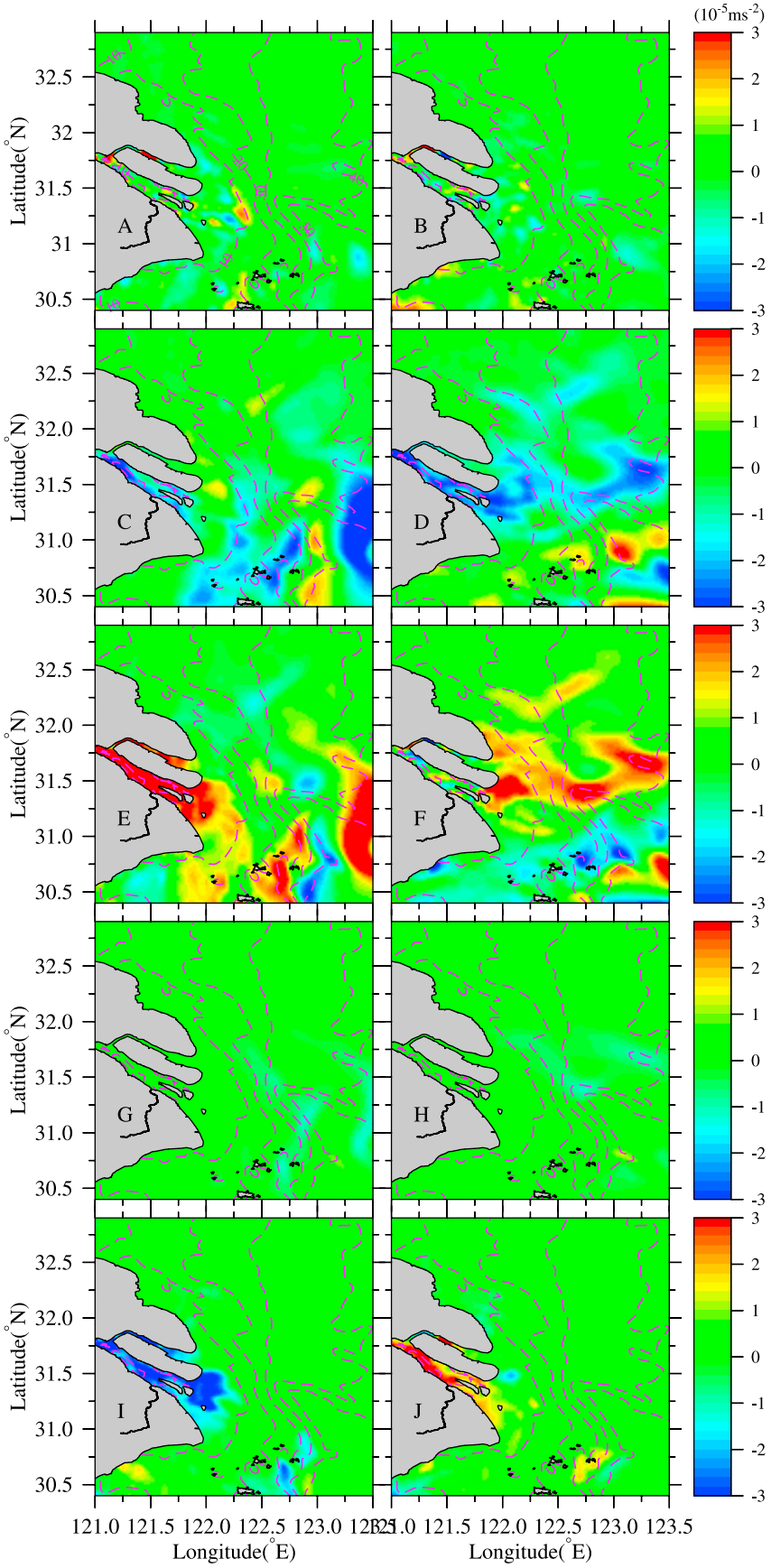
(10^-5 ms^-2)
A
B
C
D
E
F
G
H
I
J
Latitude(°N)
Longitude(°E)
32.5
32.0
31.5
31.0
30.5
121.0
121.5
122.0
122.5
123.0
123.5
3
2
1
0
-1
-2
-3

Figure 13

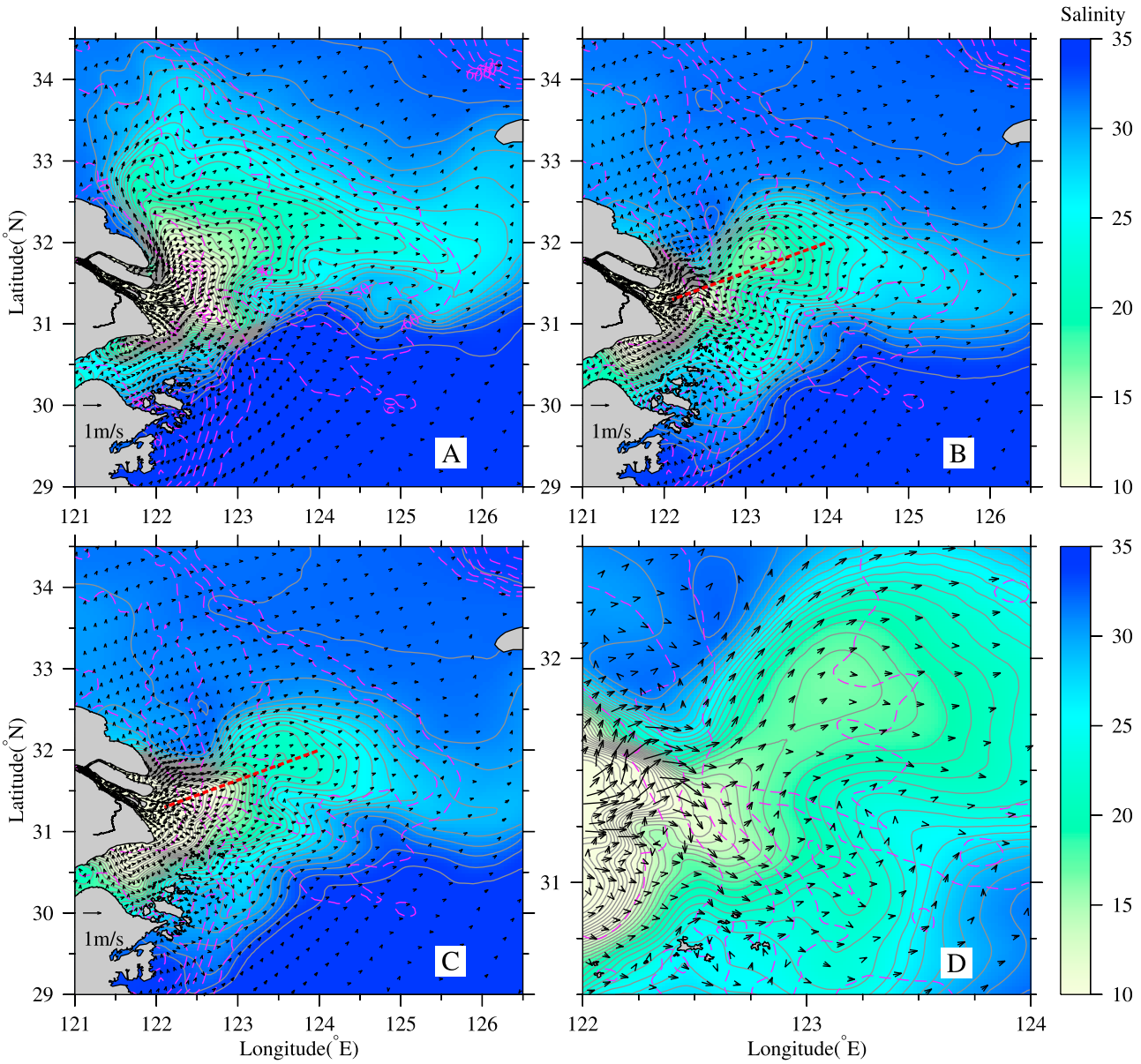

Figure 14. (a) Surface salinity and current from Exp3 and tidal-averaged surface salinity and residual current during (b) the spring tide and (c) the neap tide from Exp4. The red dashed line represents the location of the section used in Figure 15. (d) A zoom-in view of Figure 14b around the submarine canyon.

[47] A minor southeastward plume branch that originated from the near-field plume can be identified during the spring tide (Figure 14d). The bifurcation point was near the head of the submarine canyon, similar to that of Exp2. A southeastward residual current evidently occurred on the slope, which was almost the same as that of Exp2 that was resulted from the tidal rectification. Such a residual current favors the diluted water flowing southward along the Zhejiang coast. Observations confirmed that the Changjiang diluted water frequently bifurcates into two branches, one northeastward, and the other south or southeastward [*Zhu et al.*, 2003]. However, if the tide was excluded, the southward branch of the Changjiang River plume was greatly weakened, as shown in Figure 14a.

[48] During the neap tide, the freshwater extended farther east (Figure 14c), with the 10 psu isohaline reaching 122.7°E, or 20 km east to the spring tidal case. Tidally rectified residual current is proportional to the tidal range [*Loder*, 1980; *Chen and Beardsley*, 1995]. Hence similar to Exp2, the southeastward residual current on the slope almost

Figure 13. Tidal-averaged surface momentums in (a, c, e, g, i) *x* direction and (b, d, f, h, j) *y* direction during the neap tide from Exp 2. Shown are momentum advection (Figures 13a and 13b), Coriolis force (Figures 13c and 13d), barotropic gradient force (Figures 13e and 13f), baroclinic gradient force (Figures 13g and 13h), and friction (Figures 13i and 13j).

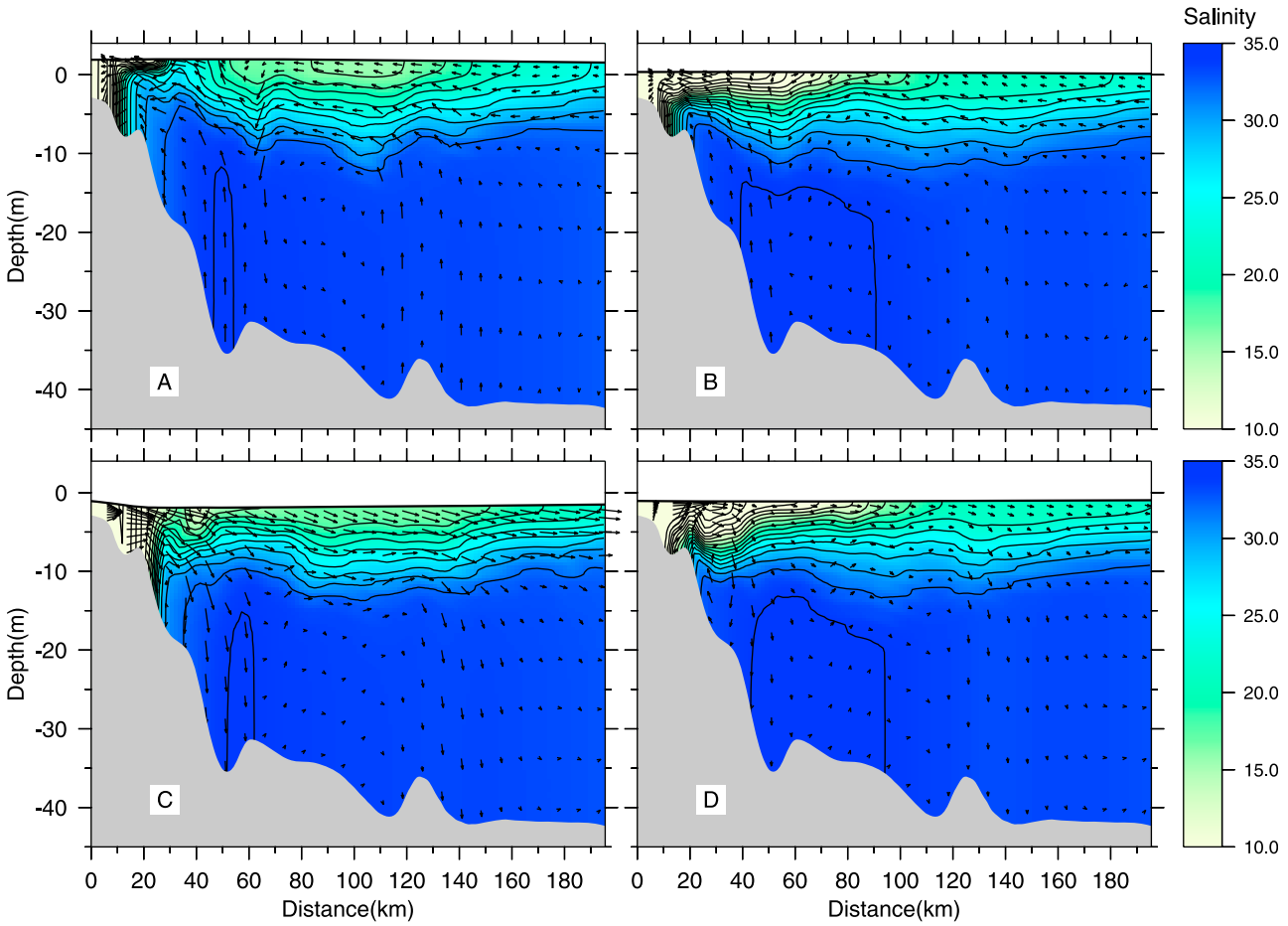

Figure 15. Sectional profiles of the salinity and velocity at (a, b) the maximum flood and (c, d) the maximum ebb during the spring tide (Figures 15a and 15c) and the neap tide (Figures 15b and 15d) from Exp4. For section location see Figure 14.

vanished due to the reduced tidal energy. The southeastward branch of the Changjiang River plume rotated to the east due to the ambient current. Therefore the southeastward branch of the Changjiang River plume is produced during the spring tide.

4.2.2. Plume Detachment

[49] A detached pulse of freshwater can be found near 123.2°E, 31.75°N during the spring tide (Figure 14d). *Moon et al.* [2010] suggested that the Changjiang River plume can be detached on the Changjiang Bank by the intensified tidal mixing during the spring tide. However, the detaching location and size of the freshwater patch in this study were different from that reported by *Moon et al.* [2010]. It was smaller and closer to the coast. Sectional salinity distributions along the mainstream of the plume at the maximum flood and ebb were shown in Figure 15 (For section location, see Figure 14). The northward shelf currents carried the saline water mass to the Changjiang River mouth and helped to maintain the high salinity in the lower water column. During the spring tide, the saline seawater climbed up strongly along with the flood current on the slope (Figure 15a). The amplitude of vertical velocity was $O(0.0007)$ m s^{-1}, resulting in a vertical tidal excursion distance of $O(10)$ m. Generally, the depth of the pycnocline was less than 10 m and its thickness was about 6 m. Therefore, the saline water can climb up to the surface during the spring tide and disconnect part of the plume (Figure 15a). Consequently, a fresher patch appeared seaward of the slope, as shown in Figure 14b.

[50] During the neap tide, because of the reduced tidal energy, the flood current became weak, and the saline water mass can hardly reach the surface (Figure 15b). Hence, the freshwater patch was less evident than the spring tide, and the plume was more stratified (Figures 15b and 15d).

5. Summary

[51] Tidal modulation on the Changjiang River plume was explored by using a numerical model that encompasses the entire Yellow Sea, East China Sea and adjacent ocean regions with higher-resolution grids around the river mouth. Skill assessments based on the model simulations forced by real observations indicated that the model is reliable to characterize the tide, shelf currents, and temporal-spatial variations of the Changjiang River plume. Comparisons of the model validation simulation with and without the tide forcing further confirmed the critical role played by the tidal modulation on the Changjiang River plume.

[52] Two idealized experiments were conducted at first, in which the wind forcing and the shelf currents were excluded. Without the tidal forcing, we found that the Changjiang River

plume strongly extends to the upstream along the Jiangsu coast, a phenomenon that has rarely been observed but frequently occurs in the model studies without the tidal forcing. When superimposing with the tide, however, the upstream extension vanishes. The large tide along the Jiangsu coast is sufficient to mix the water column, resulting in the formation of strong along-coastal salinity gradient at the north side of the Changjiang River mouth, which resists the upstream extension of the plume.

[53] The model results also showed distinguishable spatial pattern of the Changjiang River plume with respect to the spring-neap tidal variations. During the spring tide, there is a near-field plume located roughly inside the 30 m isobath. At its frontal portion, the subtidal momentum is balanced by the momentum advection and the Coriolis force via a mechanism of tidal rectification, which drives a residual current mainly to the southeast. Around the head of the submarine canyon an anticyclonically rotated plume bulge occurs, as a result of the local high of subtidal sea level that could result from the tidal asymmetry. The bulge rotates the Changjiang River plume to the northeast at about 122.5°E. Considering that the wind and the shelf currents were not included in this experiment, this indicated that the northeastward extension is an intrinsic property of the Changjiang River plume. In addition, the near-field plume and the bulge characterize a bidirectional plume structure that separated from the head of submarine canyon. While during the neap tide, because of the reduced tidal energy, the effects of the tidal rectification and the tidal asymmetry become small, therefore the near-field plume extends farther east and the bulge is less evident.

[54] Examinations by adding the external forcings of the 4 m s^{-1} southerly wind and the shelf currents indicated that, although the wind forcing ultimately drives the Changjiang River plume to the northeast in the far field, the dynamics of the tidal modulation are robustly maintained in the region near the river mouth. The near-field plume is almost identical to that without the wind forcing. Although the bulge merges into the far-field plume due to the intensified mixing, the Changjiang River plume rotates to the northeast at almost the same place as that without the wind forcing. Furthermore, the bidirectional plume structure is maintained and is even clearer. If excluding the tidal forcing, the southeastward branch disappears. We also found that during the spring tide, the bottom saline water can penetrate the river plume by the convective transport along the slope, thereby cutting off the Changjiang River plume and forming the freshwater detachment.

[55] **Acknowledgments.** The authors express sincere thanks to two anonymous reviewers for their insightful suggestions on improving the manuscript. This study was jointly supported by National Natural Science Foundation of China (grant 40806034), the Funds for Creative Research Groups of China (grant 41021064), National Natural Science Foundation of China (grant 40776012) and National Basic Research Program of China (2011CB409801). The authors also appreciate Mac Sisson for his assistance in editing the manuscript.

References

Ahsan, A. K. M. Q., and A. F. Blumberg (1999), Three-dimensional hydrothermal model of Onondaga Lake, New York, *J. Hydraul. Eng.*, *125*(9), 912–923, doi:10.1061/(ASCE)0733-9429(1999)125:9(912).

Allen, J. I., P. J. Somerfield, and F. J. Gilbert (2007), Quantifying uncertainty in high-resolution coupled hydrodynamic-ecosystem models, *J. Mar. Syst.*, *64*, 3–14, doi:10.1016/j.jmarsys.2006.02.010.

Beardsley, R. C., R. Limeburner, H. Yu, and G. A. Cannon (1985), Discharge of the Changjiang (Yangtze River) into the East China Sea, *Cont. Shelf Res.*, *4*, 57–76, doi:10.1016/0278-4343(85)90022-6.

Blumberg, A. F. (1994), A primer for ECOM-si, report, HydroQual, Mahwah, N. J.

Blumberg, A. F., and G. L. Mellor (1987), A description of a three-dimensional coastal ocean circulation model, in *Three-Dimensional Coastal Ocean Models*, *Coastal Estuarine Sci.*, vol. 4, edited by N. S. Heaps, pp. 1–16, AGU, Washington, D. C.

Chang, P. H., and A. Isobe (2003), A numerical study on the Changjiang diluted water in the Yellow and East China Seas, *J. Geophys. Res.*, *108*(C9), 3299, doi:10.1029/2002JC001749.

Chao, S. Y. (1988), River-forced estuarine plumes, *J. Phys. Oceanogr.*, *18*, 72–88, doi:10.1175/1520-0485(1988)018<0072:RFEP>2.0.CO;2.

Chao, S. Y. (1990), Tidal modulation of estuarine plumes, *J. Phys. Oceanogr.*, *20*, 1115–1123, doi:10.1175/1520-0485(1990)020<1115:TMOEP>2.0.CO;2.

Chen, C., and R. C. Beardsley (1995), A numerical study of stratified tidal rectification over finite-amplitude banks. Part I: Symmetric banks, *J. Phys. Oceanogr.*, *25*, 2090–2110, doi:10.1175/1520-0485(1995)025<2090:ANSOST>2.0.CO;2.

Chen, C., J. Zhu, E. Ralph, S. A. Green, J. W. Budd, and F. Y. Zhang (2001), Prognostic modeling studies of the Keweenaw Current in Lake Superior, part I: Formation and evolution, *J. Phys. Oceanogr.*, *31*, 379–395, doi:10.1175/1520-0485(2001)031<0379:PMSOTK>2.0.CO;2.

Chen, C., et al. (2008), Physical mechanisms for the offshore detachment of the Changjiang diluted water in the East China Sea, *J. Geophys. Res.*, *113*, C02002, doi:10.1029/2006JC003994.

Choi, B. H. (1980), A tidal model of the Yellow Sea and Eastern China Sea, *Rep*. 80-02, 72 pp., Korean Ocean Res. and Dev. Inst., Ansan, South Korea.

Editorial Board for Marine Atlas (1992), Ocean Atlas in Huanghai Sea and East China Sea (Hydrology), map, China Ocean, Beijing.

Epifanio, C. E., and R. W. Garvine (2001), Larval transport on the Atlantic continental shelf of North America: A review, *Estuarine Coastal Shelf Sci.*, *52*, 51–77, doi:10.1006/ecss.2000.0727.

Fong, D. A., and W. R. Geyer (2002), The alongshore transport of freshwater in a surface-trapped river plume, *J. Phys. Oceanogr.*, *32*, 957–972, doi:10.1175/1520-0485(2002)032<0957:TATOFI>2.0.CO;2.

Foreman, M. G. G., R. F. Henry, R. A. Walters, and V. A. Ballantyne (1993), A finite-element model for tides and resonance along the north coast of British Columbia, *J. Geophys. Res.*, *98*(C2), 2509–2531, doi:10.1029/92JC02470.

Galperin, B., L. H. Kantha, S. Hassid, and A. Rosati (1988), A quasi-equilibrium turbulent energy model for geophysical flows, *J. Atmos. Sci.*, *45*, 55–62, doi:10.1175/1520-0469(1988)045<0055:AQETEM>2.0.CO;2.

Gao, L., D. Li, and P. Ding (2009), Quasi-simultaneous observation of currents, salinity and nutrients in the Changjiang (Yangtze River) plume on the tidal timescale, *J. Mar. Syst.*, *75*, 265–279, doi:10.1016/j.jmarsys.2008.10.006.

Ge, J., P. Ding, C. Chen, and P. Xue (2008), Low-salinity plume in the Changjiang and adjacent coastal regions: A model-data comparison, in *Proceedings of the 31st International Conference of Coastal Engineering 2008*, edited by J. M. Smith, pp. 4471–4481, World Sci., Singapore.

Geyer, W. R. (1995), Tide-induced mixing in the Amazon frontal zone, *J. Geophys. Res.*, *100*(C2), 2341–2353, doi:10.1029/94JC02543.

Guo, X., and A. Valle-Levinson (2007), Tidal effects on estuarine circulation and outflow plume in the Chesapeake Bay, *Cont. Shelf Res.*, *27*, 20–42, doi:10.1016/j.csr.2006.08.009.

Horner-Devine, A. R., D. A. Jay, P. M. Orton, and E. Y. Spahn (2009), A conceptual model of the strongly tidal Columbia River plume, *J. Mar. Syst.*, *78*, 460–475, doi:10.1016/j.jmarsys.2008.11.025.

Isobe, A., M. Ando, T. Watanabe, T. Senjyu, S. Sugihara, and A. Manda (2002), Freshwater and temperature transport through the Tsushima-Korea Straits, *J. Geophys. Res.*, *107*(C7), 3065, doi:10.1029/2000JC000702.

Kim, H. C., et al. (2009), Distribution of Changjiang diluted water detected by the satellite chlorophyll-*a* and its interannual variation during 1998–2007, *J. Oceanogr.*, *65*, 129–135, doi:10.1007/s10872-009-0013-0.

Le, K. (1984), A preliminary study of the path of the Changjiang diluted water [in Chinese], *Oceanol. Limnol. Sin.*, *15*(2), 157–167.

Lee, H. J., and S. Y. Chao (2003), A climatological description of circulation in and around the East China Sea, *Deep Sea Res., Part II*, *50*, 1065–1084, doi:10.1016/S0967-0645(03)00010-9.

Lee, S. H., and R. C. Beardsley (1999), Influence of stratification on residual tidal currents in the Yellow Sea, *J. Geophys. Res.*, *104*(C7), 15,679–15,701, doi:10.1029/1999JC900108.

Li, D., J. Zhang, D. Huang, Y. Wu, and J. Liang (2002), Oxygen depletion off the Changjiang (Yangtze River) estuary, *Sci. China, Ser. D Earth Sci.*, *45*, 1137–1146, doi:10.1360/02yd9110.

Liu, Y., P. MacCready, B. M. Hickey, E. P. Dever, P. M. Kosro, and N. S. Banas (2009a), Evaluation of a coastal ocean circulation model for the Columbia River plume in summer 2004, *J. Geophys. Res.*, *114*, C00B04, doi:10.1029/2008JC004929.

Liu, Y., P. MacCready, and B. M. Hickey (2009b), Columbia River plume patterns in summer 2004 as revealed by a hindcast coastal circulation model, *Geophys. Res. Lett.*, *36*, L02601, doi:10.1029/2008GL036447.

Loder, J. W. (1980), Topographic rectification of tidal currents on the sides of Georges Bank, *J. Phys. Oceanogr.*, *10*, 1399–1416, doi:10.1175/1520-0485(1980)010<1399:TROTCO>2.0.CO;2.

Lü, X., F. Qiao, C. Xia, J. Zhu, and Y. Yuan (2006), Upwelling off the Yangtze River estuary in summer, *J. Geophys. Res.*, *111*, C11S08, doi:10.1029/2005JC003250.

Ma, C., D. Wu, X. Lin, J. Yang, and X. Ju (2010), An open-ocean forcing in the East China and Yellow Seas, *J. Geophys. Res.*, *115*, C12056, doi:10.1029/2010JC006179.

MacCready, P., N. S. Banas, B. M. Hickey, E. P. Dever, and Y. Liu (2009), A model study of tide- and wind-induced mixing in the Columbia River estuary and plume, *Cont. Shelf Res.*, *29*, 278–291, doi:10.1016/j.csr.2008.03.015.

Mao, H., Z. Gan, and S. Lan (1963), Preliminary study on the Changjiang diluted water and its mixing natures [in Chinese], *Oceanol. Limnol. Sin.*, *5*(3), 183–206.

Maréchal, D. (2004), A soil-based approach to rainfall-runoff modeling in ungauged catchments for England and Wales, Ph.D. thesis, Cranfield Univ., Cranfield, U. K.

Matano, R. P., and E. D. Palma (2010), The upstream spreading of bottom-trapped plumes, *J. Phys. Oceanogr.*, *40*, 1631–1650, doi:10.1175/2010JPO4351.1.

McCabe, R. M., P. MacCready, and B. M. Hickey (2009), Ebb-tide dynamics and spreading of a large river plume, *J. Phys. Oceanogr.*, *39*, 2839–2856, doi:10.1175/2009JPO4061.1.

Mellor, G. L., and T. Yamada (1982), Development of a turbulence closure model for geophysical fluid problem, *Rev. Geophys.*, *20*, 851–875, doi:10.1029/RG020i004p00851.

Moon, J. H., I. C. Pang, and J. H. Yong (2009), Response of the Changjiang diluted water around Jeju Island to external forcings: A modeling study of 2002 and 2006, *Cont. Shelf Res.*, *29*, 1549–1564, doi:10.1016/j.csr.2009.04.007.

Moon, J. H., N. Hirose, J. H. Yoon, and I. C. Pang (2010), Offshore detachment process of the low-salinity water around Changjiang bank in the East Chinese Sea, *J. Phys. Oceanogr.*, *40*, 1035–1053, doi:10.1175/2010JPO4167.1.

Murphy, A. H. (1988), Skill scores based on the mean square error and their relationships to the correlation coefficient, *Mon. Weather Rev.*, *116*(12), 2417–2424, doi:10.1175/1520-0493(1988)116<2417:SSBOTM>2.0.CO;2.

Narayanan, C., and R. W. Garvine (2002), Large scale buoyancy driven circulation on the continental shelf, *Dyn. Atmos. Oceans*, *36*, 125–152, doi:10.1016/S0377-0265(02)00028-3.

Nash, J. D., and J. N. Moum (2005), River plumes as a source of large-amplitude internal waves in the coastal ocean, *Nature*, *437*, 400–403, doi:10.1038/nature03936.

Nitani, H. (1972), Beginning of the Kuroshio, in Kuroshio, Its Physical Aspects, edited by H. Stommel and K. Yoshida, pp. 129–163, Univ. of Tokyo Press, Tokyo.

Pu, Y., W. Huang, and J. Xu (2002), The spreading direction change of the Changjiang River diluted water in 7~10 days [in Chinese with English abstract], *J. East China Sea*, *20*, 1–5.

Rabouille, C., et al. (2008), Comparison of hypoxia among four river-dominated ocean margins: The Changjiang (Yangtze), Mississippi, Pearl, and Rhone Rivers, *Cont. Shelf Res.*, *28*, 1527–1537, doi:10.1016/j.csr.2008.01.020.

Ralston, D. K., W. R. Geyer, and J. A. Lerczak (2010), Structure, variability, and salt flux in a strongly forced salt wedge estuary, *J. Geophys. Res.*, *115*, C06005, doi:10.1029/2009JC005806.

Shen, H., Z. Mao, and J. Zhu (Eds.) (2003), Saltwater Intrusion in the Changjiang Estuary, 175 pp., China Ocean, Beijing.

Simpson, J. H., and J. R. Hunter (1974), Fronts in the Irish Sea, *Nature*, *250*, 404–406, doi:10.1038/250404a0.

Smagorinsky, J. (1963), General circulation experiments with the primitive equations, I. The basic experiment, *Mon. Weather Rev.*, *91*, 99–164, doi:10.1175/1520-0493(1963)091<0099:GCEWTP>2.3.CO;2.

Tsimplis, M. N., R. Proctor, and R. A. Flather (1995), A two-dimensional tidal model for the Mediterranean Sea, *J. Geophys. Res.*, *100*(C8), 16,223–16,239, doi:10.1029/95JC01671.

Woods, A. W., and R. C. Beardsley (1988), On the barotropic discharge of a homogeneous fluid onto a continental shelf, *Cont. Shelf Res.*, *8*, 307–327, doi:10.1016/0278-4343(88)90035-0.

Wu, H., and J. Zhu (2010), Advection scheme with 3rd high-order spatial interpolation at the middle temporal level and its application to saltwater intrusion in the Changjiang estuary, *Ocean Modell.*, *33*, 33–51, doi:10.1016/j.ocemod.2009.12.001.

Wu, H., J. Zhu, and B. H. Choi (2010), Links between saltwater intrusion and subtidal circulation in the Changjiang estuary: A model-guided study, *Cont. Shelf Res.*, *30*, 1891–1905, doi:10.1016/j.csr.2010.09.001.

Xu, H., K. Zhang, J. Shen, and Y. Li (2010), Storm surge simulation along the U.S. East and Gulf Coasts using a multi-scale numerical model approach, *Ocean Dyn.*, *60*, 1597–1619, doi:10.1007/s10236-010-0321-3.

Yankovsky, A. E., and D. C. Chapman (1997), A simple theory for the fate of buoyant coastal discharges, *J. Phys. Oceanogr.*, *27*, 1386–1401, doi:10.1175/1520-0485(1997)027<1386:ASTFTF>2.0.CO;2.

Zhang, W. G., J. L. Wilkin, and R. J. Chant (2009), Modeling the pathways and mean dynamics of river plume dispersal in the New York Bight, *J. Phys. Oceanogr.*, *39*, 1167–1183, doi:10.1175/2008JPO4082.1.

Zhao, B. (1991), On the extension of Changjiang diluted water [in Chinese], *Acta Oceanol. Sin.*, *13*(5), 600–610.

Zhou, F., J. Xuan, X. Ni, and D. Huang (2009), A preliminary study of variations of the Changjiang diluted water between August of 1999 and 2006, *Acta Oceanol. Sin.*, *28*(6), 1–11.

Zhu, J., Y. Li, and H. Shen (1997), Numerical simulation of the wind field's impact on the expansion of the Changjiang River diluted water in summer [in Chinese with English abstract], *Oceanol. Limnol. Sin.*, *28*(1), 72–79.

Zhu, J., C. Xiao, and H. Shen (1998), Numerical model simulation of expansion of Changjiang diluted water in summer [in Chinese with English abstract], *Acta Oceanol. Sin.*, *20*, 13–22.

Zhu, J., P. Ding, and D. Hu (2003), Observation of the diluted water and plume front off the Changjiang River estuary during august 2000 [in Chinese with English abstract], *Oceanol. Limnol. Sin.*, *34*(3), 249–255.

Zhu, S., J. Zhu, and W. Sha (1999), A numerical study on the impact of M_2 tide on the expansion of the Changjiang River diluted water in summer [in Chinese with English abstract], *Oceanol. Limnol. Sin.*, *30*(6), 711–718.

J. Shen and H. Wang, Virginia Institute of Marine Science, School of Marine Science, College of William and Mary, Gloucester Point, VA 23062, USA.

H. Wu and J. Zhu, State Key Laboratory of Estuarine and Coastal Research, East China Normal University, Shanghai, 200062, China. (hwu@sklec.ecnu.edu.cn)